Am J Cancer Res 2021;11(2):590-617
www.ajcr.us /ISSN:2156-6976/ajcr0121773

Original Article

P4HA1 as an unfavorable prognostic marker promotes cell migration and invasion of glioblastoma via inducing EMT process under hypoxia microenvironment

Xiaosan Zhu[1*], Shanshan Liu[1*], Xueou Yang[1], Wenjun Wang[1], Wei Shao[1], Tianhai Ji[1,2]

[1]Chenggong Hospital, Xiamen University, Xiamen 361003, China; [2]Ninth People's Hospital, Shanghai Jiaotong University School of Medicine, Shanghai 200011, China. [*]Equal contributors and co-first authors.

Received September 5, 2020; Accepted December 30, 2020; Epub February 1, 2021; Published February 15, 2021

Abstract: This study aims to explore the mechanism of glioblastoma multiforme (GBM) in hypoxia through metabolomic and proteomic analysis. We showed that the migration and invasiveness of LN18 cells was significantly enhanced after 24 h of hypoxia treatment. The metabolomic and proteomic profiling were conducted in LN18 cells cultured under hypoxia condition. Correlation analysis between significant differential metabolites and proteins revealed seven proteins and ten metabolites, of which metabolite L-Arg was negatively correlated with P4HA1 protein. Meanwhile, the expression of HIF1α, nNOS and P4HA1 was up-regulated, and the concentration of L-Arg and NO was decreased and increased respectively. Knockdown of HIF1α reduced the expression of nNOS and P4HA1, the concentration of NO and the invasiveness of cells, while increased the concentration of L-Arg. Similar changes on P4HA1 expression, the concentration of L-Arg and NO were observed when the expression of nNOS was disrupted. Lastly, knockdown of P4HA1 impaired the invasion of LN18 and T98G cells, probably through regulating the expression of Vimentin, MMP2, MMP9, Snail and E-cadherin. Consistent trends on both the overexpression of these relevant genes, as well as the concentration of L-Arg and NO were also observed in all our overexpression experiments. Besides, we investigated the relationship between P4HA1 expression and prognosis by MTA, CGGA and TCGA databases. Increased P4HA1 level was correlated poor prognosis with advanced histological grade. In summary, we found that hypoxia promotes the migration and invasion of GBM via the L-Arg/P4HA1 axis which maybe an effective molecular marker or predictor of clinical outcome in GBM patients.

Keywords: Hypoxia, migration, invasion, glioblastoma multiforme, P4HA1, prognosis

Introduction

Glioblastoma multiforme (GBM) is the most common primary malignant tumor in the central nervous system [1]. Widespread invasive growth is one of the most important characteristics in GBM, which results in blurring boundary between tumor cells and surrounding normal brain tissue. This feature explains the difficulty of complete removal of the tumor tissue during surgery, and thus high recurrence rate afterwards. The average survival of GBM patients is only about 1 year with routine radiotherapy and chemotherapy after surgery treatment [2-4]. Therefore, understanding the mechanism of GBM invasiveness is critical for designing effective therapeutic interventions. Numerous studies have shown that hypoxic microenvironment plays important roles in determining GBM invasiveness, along with other intrinsic properties of cancerous cells. GBM obtains oxygen and nutrients through the diffusion of new blood vessels. As the tumor enlarges, the neovascular tumors expand, distort, and mutate abnormally. The increase of the oxygen diffusion distance in the blood vessels induces hypoxia in GBM [5, 6]. It has been reported that hypoxia causes phenotypic alteration of glioblastoma from perspectives ranging from genomics, transcriptomics, proteomics to metabolomics. Chen et al. used a three-dimensional hydrogel method to find that hypoxia can stimulate glioblastoma invasion by affecting matrix composition and metabolic

reprogramming [7]. Gagner et al. found that hypoxia promotes invasion and migration of glioblastoma by activating HIF1α, chemokine CXC motif receptor 4 (CXCR4), and expression of other hypoxia response elements [8]. Although it is known that glioblastoma prefer to reside in a relatively hypoxic environment, which accelerates its invasiveness, the explicit biological mechanism remains a mystery. Previously, studies of the effects of hypoxia on glioblastoma phenotype have been focused on understanding the functions of single genes, such as HIF1α, etc [9-11], These kind of research could not assess the influence of molecular biological changes of GBM cells at the systems level, thus severely limit the understanding of how hypoxia triggers cancer cell spreading, and further prevent the pace of targeted drug development for clinical treatment. Currently, integrative multi-omics research has become one of the most powerful tools for exploration of mechanisms under tumorigenesis and progression [12-14]. Among those methodology, proteomic and metabolic analysis have their own advantage to facilitate the discovery of proteins and metabolite components that reflect the nutrition and state of cancerous cells, as well as reveal the network interactions of the underlying mechanism [15-17].

To identify the key players that mediate the cell migration and invasion of glioblastoma in hypoxic microenvironment, we carried out the metabolic and proteomic profiling on glioblastoma cell lines under hypoxia conditions. The analysis identified significant differential metabolites and proteins that enhance the migration and invasion of the glioblastoma on hypoxia. Subsequencially, we investigated the downstream targets of these individual genes and metabolites, and how they cooperate together to stimulate the migration and invasion of glioblastoma.

Moreover, we investigated the expression of P4HA1 by immunohistochemistry (IHC) on a tissue microarray (TMA) including 128 glioma specimens and investigated its association with the survival outcome. Besides, we selected 975 and 652 glioma patients from Chinese Glioma Genome Atlas (CGGA) and The Cancer Genome Atlas (TCGA) databases, separately. Our findings provide strong evidence that cytoplasmic P4HA1 expression is a prognostic marker and a promising therapeutic target in GBM.

Materials and methods

Cell culture

The human malignant glioma cell line, LN18, was purchased from ATCC. The T98G cell lines were kindly provided by Professor Yifang PING (Institute of Pathology & Southwest Cancer Center, Southwest Hospital, Army Medical University, China). The authenticity of these cell lines was confirmed by the STR profiling analysis. The cells in the control group were cultured in a medium consisting of 90% Dulbecco's Modified Eagle Medium (DMEM) with 10% fetal bovine serum in a humidified atmosphere of 5% CO_2 at 37°C. The cells in the hypoxia group were initially cultured under the same condition as the control group for 12 h and then transferred to an incubator with 5% CO_2, 1% O_2 and 94% N_2 at 37°C.

Wound-healing assay

LN18 cell lines were seeded into 12-well plates precoated with Matrigel and allowed to migrate through a polycarbonate membrane in normoxia (37°C and 5% CO_2) or hypoxia (37°C, 1% O_2, 5% CO_2, and 94% N_2) chambers for 12 h, 24 h, 48 h and 72 h. LN18 and T98G cell lines were transfected with NC P4HA1 and siP4HA1 and grown to normoxia or hypoxia chamber for 24 h, separately. Images were taken after wounding, and the distance between the wound edges was measured using the TCapture on images captured with the SDC-500 microscope of 40×. The experiments were performed in triplicate and repeated three times.

Transwell migration assay

Log phase growth LN18 and T98G cell lines were seeded into 24-well plates with transwell chamber precoated with Matrigel and allowed to migrate through a polycarbonate membrane in normoxia (37°C, 21% O_2, 5% CO_2 and 94% N_2) or hypoxia (37°C, 1% O_2, 5% CO_2 and 94% N_2) for 12 h, 24 h, 48 h and 72 h, separately. LN18 and T98G cell lines were transfected with NC P4HA1 and siP4HA1 and grown to normoxia or hypoxia chamber for 24 h, separately. After the treatment, the transwell insert was

removed from the plate and remaining media and the cells were carefully wiped out. Then the chamber was placed into methanol to for cell fixation, followed by crystal violet staining. Then the membrane was dipped into distilled water to remove the excess crystal violet. The dried membrane then was examined under a microscope and the number of cells were counted for the migrated cells through the transwell membrane. The experiments were performed in triplicate and repeated three times.

Metabolomics analysis

The LN18 cells were cultured for 24 h under normoxia or hypoxia condition before harvest. The cells were then resuspended in 200 μl deionized water and 40 μl of the total volume was transferred to a new eppendorf tube. Repeat this step 6 times. To each tube, carefully added a stainless steel bead following 120 μl methanol (-80°C) and homogenized the samples at 60 Hz for 4 min using the TissueLyser (Shanghai Jingxin Industrial Development Co., Ltd., China). The homogeneous mixture was stored at -20°C for precipitation overnight before centrifugation. 10 μl of the aqueous layer was loaded on high-resolution tandem mass spectrometer Xevo G2 XS QTOF (Waters, UK) to detect the metabolites. The detailed parameters were described previously [18].

Proteomics analysis

The LN18 cells were cultured for 24 h under normoxia or hypoxia condition before harvest. The cells were lysed in 8 M Urea, 30 mM HEPES, 1 mM PMSF, 2 mM EDTA, 10 mM DTT and sonicated for protein extraction. After centrifugation, the supernatant was solubilized with DTT to 10 mM and incubated at 56°C for 1 h. Following incubation, in each sample, 55 mM IAA (IAM) was added, and the samples were alkylated for 1 h in the dark at room temperature. After that, 20 ug protein extraction from each sample were loaded in 10 k MWCO (Millipore) for rapid protein concentration. 200 μL of 25 mM NH_4HCO_3 was added for the second round of centrifugation. The concentrated protein was subjected to digestion with 0.9 μg trypsin at 37°C for 24 h. Dry the digested sample to completion using the SpeedVac. Peptides were dissolved in 0.1% formic acid and analyzed using Q-Exactive mass spectrometer (Thermo Fisher) as described by the manual of the machine.

MRM analysis

For the MRM confirmation, total protein was extracted from LN18 and T98G cells culture under both normoxia and hypoxia conditions after 24 h. 1 μg of trypsin was added to 30 μg of each protein solution for digestion at 37°C for 24 h. The digests were dried and each precipitate was dissolved and pooled together at 0.5 μg per sample. 2 μg of the mixed peptides was subjected to Sciex QTRAP 6500 for identification. The raw mass data were processed with Proteome Discover 1.3 (Thermo Fisher Scientific) and searched with MASCOT 2.3.01 (Matrix Science, London, U.K.) against uniprot_human_9606. The targeted peptides of the corresponding proteins were filtered and extracted using Skyline. The average area value of all peptide peak from the same protein was used to indicate the protein abundance.

Plasmid and transfection

LN18 and T98G cells were cultured to 85%-90% confluency and lipofectamine-2000 (Invitrogen, Carlsbad, CA, USA) was employed for transfection. For each target gene, both siRNA and one scrambled siRNA as control were included. The knockdown efficiency was evaluated after 48 h of transfection. The sequences of small interfering RNA (siRNA) targeting HIF1α, nNOS or P4HA1 and its negative control siRNA (NC) containing scrambled sequences are listed as follows: siHIF1α-1 sense: UAUUUGUUCACAUUAUCAGdtdt; siHIF1α-1 antisense: CUGAUAAUGUGAACAAAUAdtdt; siHIF1α-2 sense: AAUAAGAAAAUUUCAUAUCdtdt; siHIF1α-2 antisense: GAUAUGAAAUUUUCUUAUUdtdt; NC HIF1α sense: UGUUAUCACAUUCAUGUAUTT; NC HIF1α antisense: AUACAUAAUGAUGAUAACATT; sinNOS-1 sense: GUCAUUAGCAGUAGACAGAdtdt; sinNOS-1 antisense: UCUGUCUACUGCUAAUGACdtdt; sinNOS-2 sense: CAGAAUACAGGCUGACGAUdtdt; sinNOS-2 antisense: AUCGUCAGCCUGUAUUCUdtdt; NC nNOS sense: UUCUCCGAACGUGUCACGUTT; NC nNOS antisense: ACGUGACACGUUCGGAGAATT; siP4HA1-1 sense: UUUUAUUUGUUCUAACUUGdtdt; siP4HA1-1 antisense: CAAGUUAGAACAAAUAAAAdtdt; siP4HA1-2 sense: AAUUUGAAUGCAUUUACUGdtdt; siP4HA1-2 antisense: CAGUAAAUGCAUUCAAAUUdtdt; NC P4HA1 sense: AAUUACUGUU-

CAAUAUUGTT; NC P4HA1 antisense: CAAUAUUGAACAGTAAUUTT.

Construction of overexpression plasmid

The overexpression plasmids were constructed through PCR by using the following primers for each gene: HIF1α: forward-CGCGGATCCATGTGTGAGGTGATGCCCACAAT; reverse-CGCGGCCGCTATGGCCGACGTCGACCTAGTCCCGGAAGGCGGAGA; nNOS: forward-CCCAAGCTTATGTCCCTCTCTTCTCTCTGTCCTG; reverse-CCGCAATTCCTACACGGCGATCTCATCATCC; P4HA1: forward-CCCAAGCTTATGATCTGGTATATATTAATTATAGGAATTCTGCTTC; reverse-CCCTCGAGCCAAAGACTGGGGAAGCAGAATTC. The accuracy of the cDNA sequence was confirmed by sequencing.

qRT-PCR

LN18, T98G and transfected cells in both control and hypoxia groups were harvested for RNA extraction. Total RNA was isolated by TRIzol (Invitrogen, Grand Island, NY, USA) according to the manufacturer's instructions, and 1 μg RNA was converted to cDNA using the Superscript III First-Strand Synthesis System (Invitrogen). The following primer sets were used for RT-PCR: HIF1α-F: AGTGTACCCTAACTAGCCG; HIF-1α-R: CACAAATCAGCACCAAGC; nNOS-F: ATCCGCTACGCTGGCTAC; nNOS-R: GATGGGAACTTCCAACACC; P4HA1-F: GGAACAAGCCCTAAGGCAACT; P4HA1-R: TGGCAGGTAATCCACAGCAAC; β-actin-F: ATCCGCTACGCTGGCTAC; β-actin-R: CTGGAGGAATCTGGAAGAGC. The RT-PCR products (5 ul) were resolved on a 2% agarose gel and visualized by ethidium bromide staining. The experiments were performed in triplicate and repeated three times.

Western blot

For preparing the whole-cell extract, cells were harvested and lysed in RIPA buffer containing 50 mM Tris-HCl [pH 7.4], 1% Nonidet P-40, 0.25% sodium deoxycholate, 150 mM NaCl, 1 mM EDTA, 1 mM PMSF, 1 mg/ml aprotinin, 1 mg/ml leupeptin, 1 mg/ml pepstatin, 1 mM Na_3VO_4, and 1 mM NaF. Protein concentration of the lysate was quantified by the use of BCA Kit. Cell lysates were loaded onto an SDS-PAGE gel and separated by electrophoresis. After transfer of the proteins onto a piece of nitrocellulose membrane, the target molecules were detected by Western blotting using corresponding primary Abs HIF1α, P4HA1, E-cadherin, MMP2, MMP9, Snail Ab (Proteintech), GAPDH, Tubulin and nNOS Ab (Cell Signaling) and Vimentin Ab (Arigo), HRP-conjugated secondary Ab (Proteintech), and an ECL Detection kit (Thermo Pierce). Quantification of protein expression levels was performed using Image J from NIH. The experiments were performed in triplicate and repeated three times.

Quantification of L-Arg and NO concentration

LN18, T98G and transfected cells were cultured in both normoxia and hypoxia conditions with the presence of various concentrations of L-Arg and sodium nitroprusside (Selleck Chemicals). The cells were harvested after 24 h and lysed on ice for 30 min (100 μL lysis buffer/million cells). The lysate was mixed with reagents from L-Arginine assay kit (JianglaiBio) or nitric oxide assay kit (AmyJet Scientific Inc.) according to the manufacturer's instructions. The L-Arg and NO concentration was determined by fluorometric absorbance at 540 nm on spectrometer. The experiments were performed in triplicate and repeated three times.

Tissue microarray and immunohistochemistry

The protocol of the study was approved by the ethics committee at the Chenggong Hospital Affiliated to Xiamen University, General Hospital of Central War Zone and The Ninth People's Hospital, Shanghai Jiaotong University School of Medicine. The glioma tissue microarray was provided by above mentioned hospitals. Written informed consent was obtained from all patients and/or family members. A rabbit polyclonal anti-P4HA1 antibody (1:200, Proteintech) was used for immunohistochemistry staining according to its instruction. All sections were scored by two independent pathologists in a blinded fashion. In particular, the intensity of positive staining in the cytoplasm was scored on a scale of 0-3 (0: negative; 1: light brown; 2: medium brown; 3: dark brown). The percentage of positive staining cells was scored as 1 (1-25%), 2 (26-50%), 3 (51-75%) and 4 (76-100%). When duplicated cores show different staining, the higher score from the two tissue cores was taken as the immune reactivity score (IRS) [19]. The final score was calculated by multiplying the scores of staining intensity and the percentage of

positive cells. Based on IRS, P4HA1 staining pattern was defined as: low (IRS: 0-7) and high (IRS: 8-12).

CGGA and TCGA data proceeding

Gene expression and glioma patient survival data were downloaded from the TCGA (www.cancaergenome.nih.gov) and the CGGA (www.cgga.org.cn). The CGGA and TCGA database provides multiple types of data of 975 and 652 glioblastoma cases. The expression value of P4HA1 was classified as either high or low. Survival probability was calculated in days from the date of diagnosis to the time of death.

Statistic analysis

All data was analysed by GraphPad Prism 5 software and expressed as the mean ± standard deviation (SD). Statistically significant differences between groups were determined by one-way analysis of variance (ANOVA), wilcox. test, pearson correlation analysis and unpaired two-sample Student's t-test. Other statistical computations and figures drawing were performed with several packages in the statistical software environment R, version 3.3.2. ANOVA was employed to determine the difference of P4HA1 expression among gliomas with varied histological grades. OS curve was plotted with Kaplan-Meier method. All results were considered to be statistically significant at $P<0.05$.

Results

Hypoxia increases the migration and invasiveness of glioblastoma

To determine how the invasiveness of glioblastoma is affected by the oxygen content in the environment, we carried out the cell migration and invasion assays on LN18 cell lines cultured under both hypoxic and normoxic condition for 12 h, 24 h, 48 h and 72 h. It is clear that migration distance of cells under hypoxia was longer than that under normoxia starting from 24 h, and continue to increase until 72 h. No migration difference was observed within 12 h (**Figure 1A** and **1C**), indicating that hypoxia could remarkably enhance the migration of LN18 cells. To check the invasion of glioblastoma under hypoxia, in vitro assay was carried out on LN18 cell lines. The increased invasion is consistent with previous studies, although with some variation, which may be due to the different cell types [19, 20]. There was no significant difference of cell invasiveness observed at 12 h between hypoxic and normoxic conditions. Increased cell invasion was seen under hypoxia from 24 h and continue to boost for the next 48 h (**Figure 1B** and **1D**). For the rest of our study, we mainly focused on the 24 h time point as it is the earliest onset we observed for different migration phenotypes and recent publication also followed the same time window to investigate systematic response to hypoxia in glioblastoma cell lines [21].

Profiling the metabolome of glioblastoma under hypoxia and normoxia

To identify the core metabolites associated with hypoxia induced cell invasion, we performed the liquid chromatography-mass spectrometry (LC-MS) to profile the metabolome on hypoxic LN18 cells. Six replicates were included to reduce the bias and variabilities in the experimental process. Using the student's t-test, we identified 564 down-regulated and 596 up-regulated metabolites under hypoxia in the negative mode, as well as 901 up-regulated and 1,057 down-regulated metabolites in the positive mode (**Figure 2A**, **2B** and Table S1). The principal component analysis (PCA) reveals that the metabolome of LN18 cells undergo remarkable changes under hypoxia compared to normoxia, as samples from the two groups are well separated from the first two PCs (**Figure 2C** and **2D**). Using these differential metabolites, we conducted the hierarchical clustering analysis. In **Figure 2E** and **2F**, we show the drastic difference in metabolic profile between normoxia and hypoxia, while the variances between replicates are negligible. The identified metabolites include many known molecules related to hypoxia or tumor invasion. For example, we successfully identified 4-hydroxyproline, reported as a metabolic marker in hypoxic cancer cells [22]. To systematically validate the hypoxia related metabolomes discovered here, we carried out literature search in the top seventy metabolites. Eight of them (11%) have been shown associated with hypoxia response, while another six (9%) have been indicated in relation to tumor invasion and metastasis. Last, four of the metabolites (6%) have been reported to function in hypoxia-induced tumor migration [23,

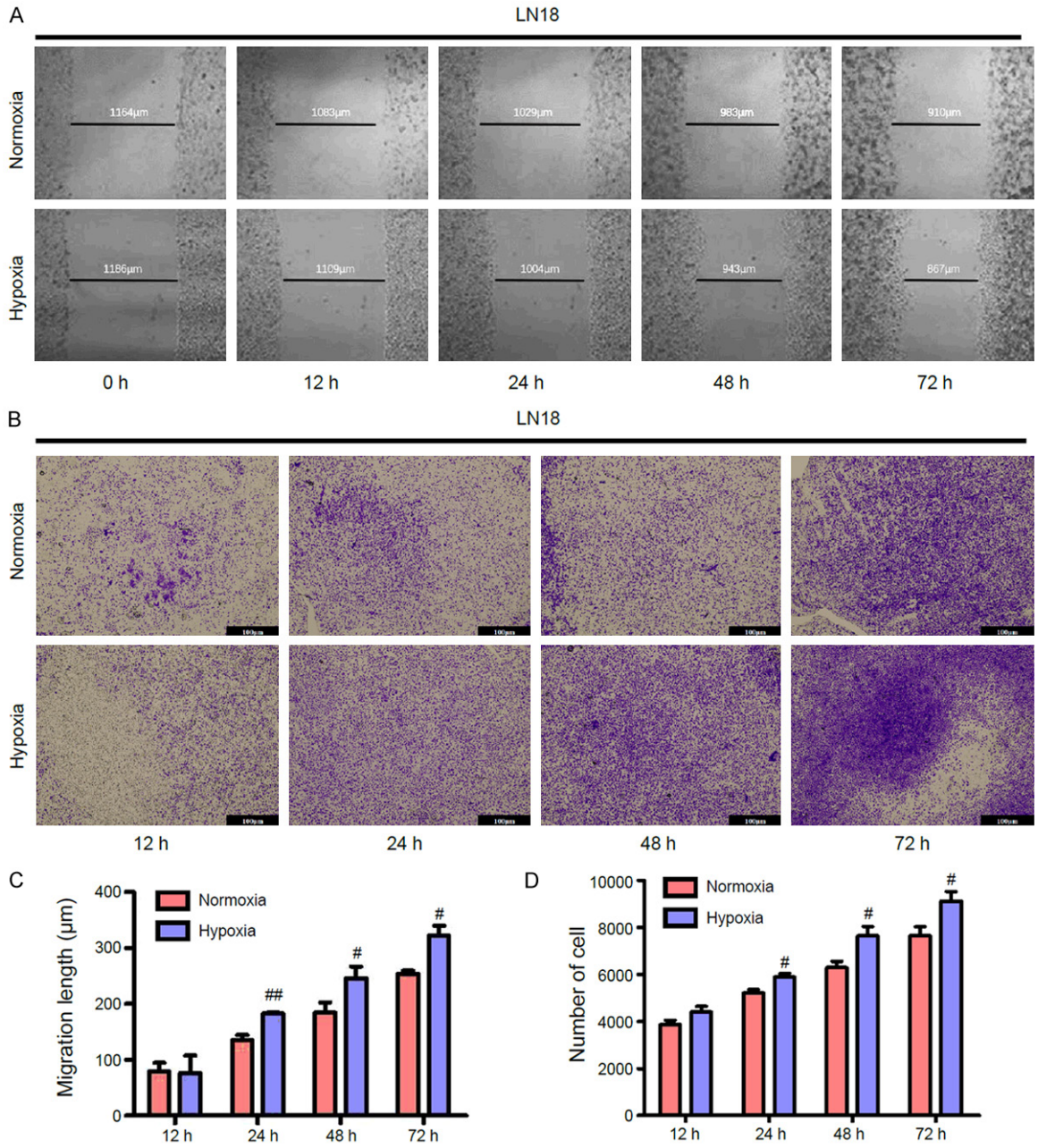

Figure 1. Hypoxia enhances glioblastoma cell migration and invasion. A, C. Wound-healing assays revealed the migration activity of LN18 cells in response to hypoxia in time course from 12 h up to 72 h. B, D. Transwell migration assay revealed the invasion activity of LN18 cells in response to hypoxia in time course from 12 h up to 72 h. Results are presented as mean ± SD; n=3; # comparison of hypoxia to normoxia, ##0.01<P<0.05, #P<0.05, one-way ANOVA test.

24]. These results suggest that metabolic changes may be an important factor in hypoxia induced cell invasion.

Profiling the proteome of glioblastoma under hypoxia and normoxia

We further performed the proteomic profiling of LN18 cells under normoxia and hypoxia to identify the major players during glioblastoma progression in response to hypoxia. Nine replicates from normoxic and hypoxic conditions were included. The two groups displayed clear separation according to the first two PCs (**Figure 3A**). Within a total of 2,348 quantifiable proteins, the abundance of 62 proteins is found to be significant altered (FDR<0.05 and fold change >1.5 or <0.67) (**Figure 3B**), including 28

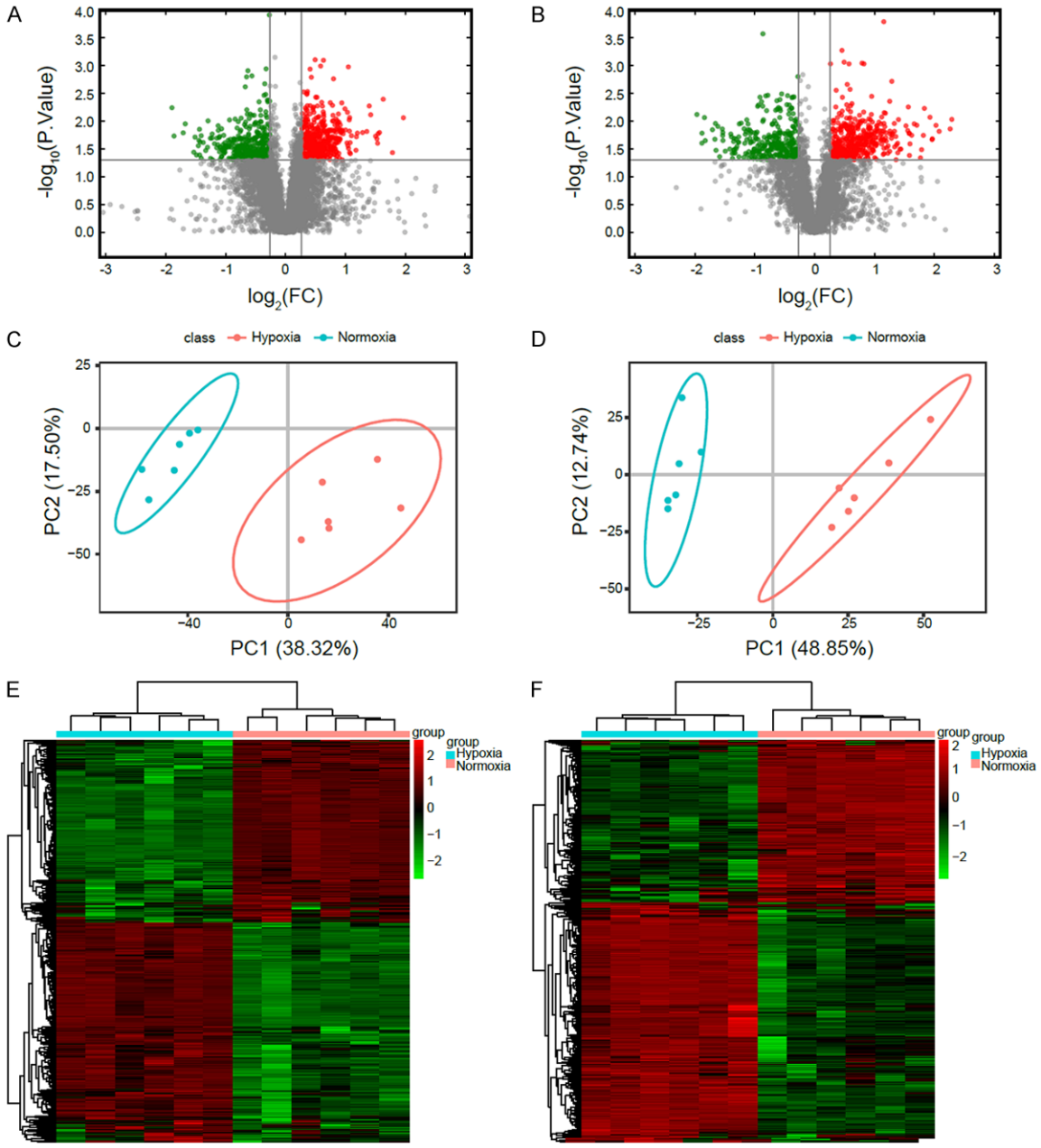

Figure 2. Overview of metabolic alternation in hypoxic glioblastoma cells. A, B. The altered metabolites in positive and negative modes are visualized in volcano plot. Up and down regulated metabolites are shown in red and green respectively. C, D. PCA analysis is performed to visualize the general clustering trends of positive and negative metabolites among the 12 experimental groups. Clear segregation of metabolic profiles was shown between hypoxia and normoxia groups. E, F. Heat maps show the hierarchical clustering analysis of the dataset consisted of metabolites quantified in all 12 samples in either positive or negative mode.

up-regulated proteins and 34 down-regulated proteins, which were listed in Table S2. In **Figure 3C**, we show the drastic difference in proteomic profile between normoxia and hypoxia, while the variances between replicates are negligible. Among these differentially expressed proteins, 27 (44%) have been demonstrated to be involved in hypoxia responses and up to 28 (45%) are related to tumor invasion [25-27]. 21 of them (34%) are associated with both biological processes, such as P4HA1 and P4HA2 [28-30]. To define the signaling pathways correlated with these proteins, we conducted GO term enrichment analysis. The top pathways that

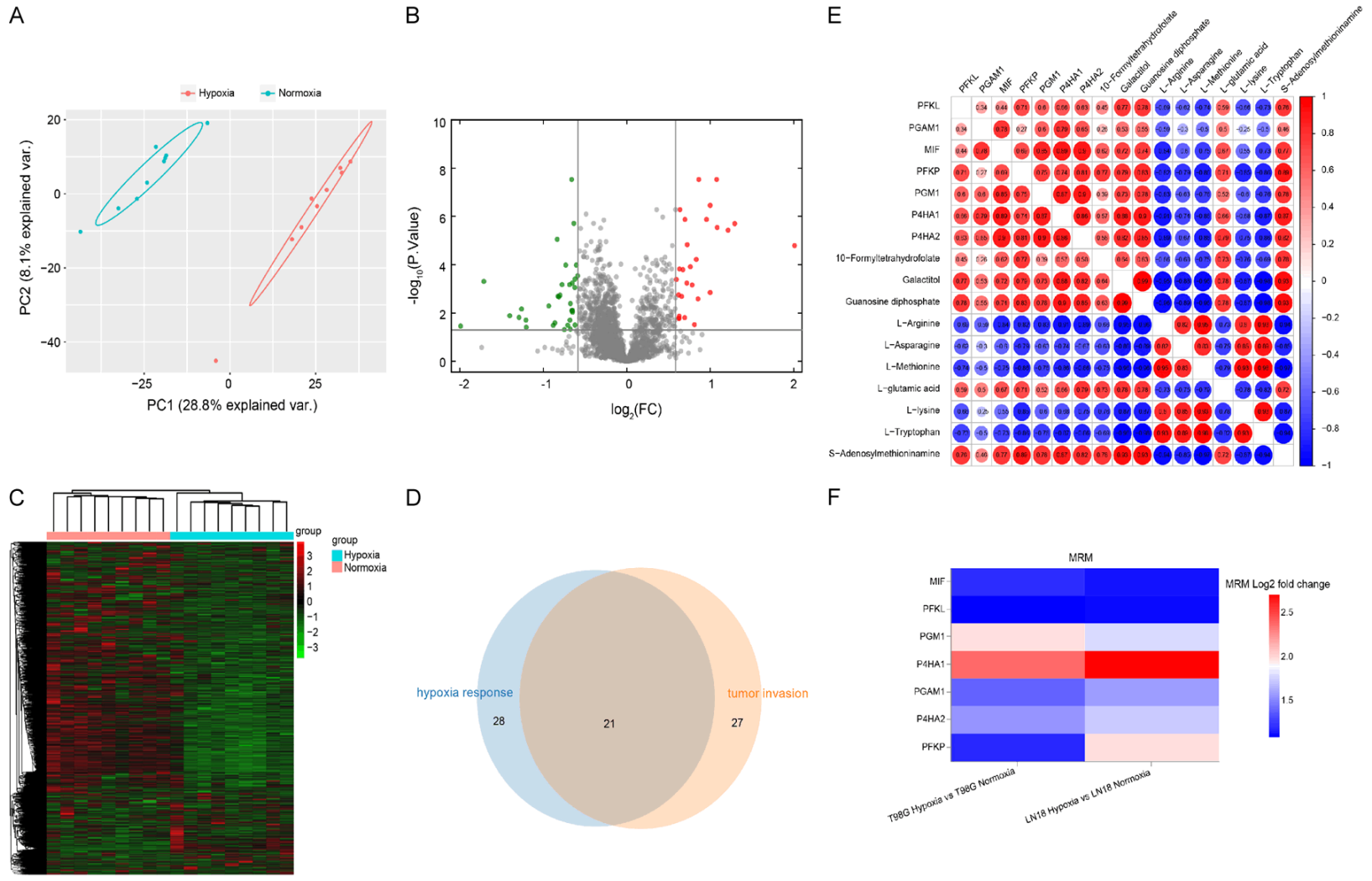

Figure 3. The landscape of differentially expressed proteins in response to hypoxia and integrative analysis reveals critical genes and metabolites of hypoxic response in glioblastoma. A. PCA analysis is performed to visualize the general clustering trends among the 18 experimental groups. There is clear segregation of the protein profiles of the hypoxia group from the normoxia group. B. Differentially expressed proteins are visualized in volcano plot. Grey dots represent proteins without significant change, while the red and green dots denote up and down regulated proteins respectively. C. Heat map shows the hierarchical clustering analysis of the dataset consisted of proteins quantified in the 18 samples. D. Venn diagram for numbers of differentially expressed proteins associated with hypoxia or tumor invasion. E. A matrix of pairwise pearson correlations is shown between the 7 differentially expression proteins and 10 altered metabolites identified from integrative analysis. Red and blue dots indicate positive and negative correlation respectively. The numbers in the dots represent the pearson correlation scores. F. MRM assays confirmed the expression of the 7 proteins in both LN18 and T98G cell lines. Color intensity represents the log2 fold changes.

stand out are those involved in biological process, such as pyridine-containing compound metabolic process and ATP metabolic process. Both pathways contain at least 5 or 6 differentially expressed proteins. The significantly altered proteins are also classified into pathways including cell junction, carbohydrate binding and monosaccharide binding, etc (**Figure 3D**). When searching against KEGG database, we identified 8 significant signaling pathways ($P<0.05$) that all fall into the category of biosynthesis and cellular metabolism (Table S3).

Integrated analysis identifies key proteins and metabolites involved in hypoxia induced tumor migration

So far, we have identified a large number of metabolites and proteins associated with tumor cell invasion in response to hypoxia. To narrow down the list on the ones that are most relevant to the physiological process, we screened out those population by performing integrative analysis to identify the key pathways involved in hypoxia using both differential expressed proteins and metabolites. This analysis resulted in nine commonly enriched pathways (galactose metabolism, biosynthesis of amino acids, carbon metabolism, arginine and proline metabolism, fructose and mannose metabolism, biosynthesis of amino acids, carbon metabolism and arginine and proline metabolism). Then we found the significantly changed metabolites and proteins associated with these pathways. In summary, a total of 10 metabolites were identified. They are 10-Formyltetrahydrofolate, Galactitol, Guanosine diphosphate, L-Arginine, L-Asparagine, L-Methionine, L-glutamic acid, L-lysine, L-Tryptophan and S-Adenosylmethioninamine. The list of proteins includes MIF, PFKL, PGM1, P4HA1, PGAM1, P4HA2 and PFKP. To investigate the relation between the differentially expressed genes and the significantly altered metabolites, we calculated the pairwise Pearson's correlation scores using their relative quantification. The matrix of correlation scores showed that the seven proteins are positive-correlated with 10-Formyltetrahydrofolate, Galactitol, Guanosine diphosphate, L-glutamic acid and S-Adenosylmethioninamine. On the other hand, they are anti-correlated with L-Arginine, L-Asparagine, L-Methionine, L-lysine and L-Tryptophan (**Figure 3E**).

We selected the seven differential expressed proteins to validate the result using multiple reaction monitoring (MRM) experiments. Using two glioblastoma cell lines, LN18 and T98G, we show that all the proteins are consistently up-regulated under hypoxia in both cell lines (**Figure 3F**). Among those, P4HA1 has the highest increase of its expression and it has the strongest negative correlation with L-Arginine (L-Arg). Together, these results help us to narrow down the number of both differentially expression protein and its correlated metabolites and we sought to continue studying the molecular mechanism of how P4HA1 and L-Arg affect glioblastoma cell line migration under hypoxic conditions.

Effect of hypoxia on the P4HA1 expression and L-Arg production

To confirm the up-regulation of P4HA1 under hypoxic conditions and its negative correlation with L-Arg, we first assured that hypoxia enhanced migration was also observed in both LN18 and T98G cells (**Figure 4A**). The same effect was noticed on cell invasion. Both LN18 and T98G cells showed an increased invasion activity when treated under hypoxia condition (**Figure 4B**). Then we examined expression of P4HA1 and L-Arg concentration in both LN18 and T98G cell lines in response to hypoxia. Consistent with the results of proteomic and MRM analysis, the expression of P4HA1 was significantly increased, with its mRNA induced at approximately 2-fold and protein at 1.2-fold (**Figure 4B** and **4C**). In contrast, the concentration of cellular L-Arg decreased by half when exposed to 1% O_2 for 24 h (**Figure 4D**).

We further assessed the expression and concentration levels of several other genes or molecules that have been implicated in hypoxia-induced tumor progression. HIF1α is a transcription factor that promotes extracellular matrix remodeling under hypoxic conditions by inducing P4HA1 and its activation is regulated by PI3k/Akt signaling pathway [24, 31]. Elevated level of HIF1α is associated with cancer progression [32]. Indeed, we found that the upregulation of P4HA1 in hypoxic cells is associated with elevated expression of HIF1α (**Figure 4B** and **4C**). A similar trend was observed on the expression of nNOS at both mRNA and protein levels. nNOS is another known hypoxia-dependent factor, of which the expression level is HIF1α-dependent in neuroblastoma cells [33]. The NOSs family are key cellular enzymes for L-Arg catalyzation, and the produced nitric

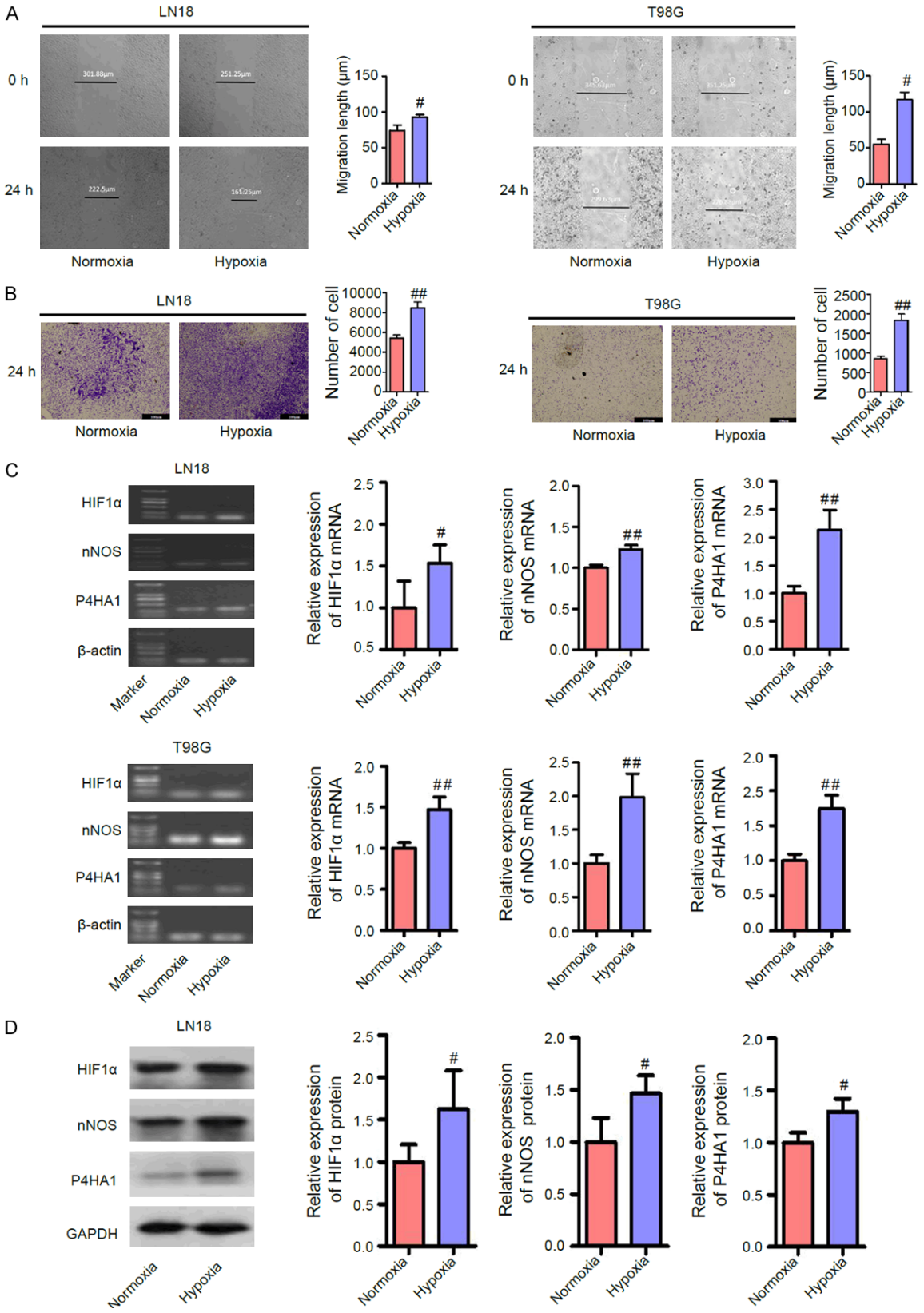
A
LN18
T98G
0 h
24 h
Normoxia
Hypoxia
Migration length (μm)
B
Number of cell
C
HIF1α
nNOS
P4HA1
β-actin
Marker
Relative expression of HIF1α mRNA
Relative expression of nNOS mRNA
Relative expression of P4HA1 mRNA
D
GAPDH
Relative expression of HIF1α protein
Relative expression of nNOS protein
Relative expression of P4HA1 protein

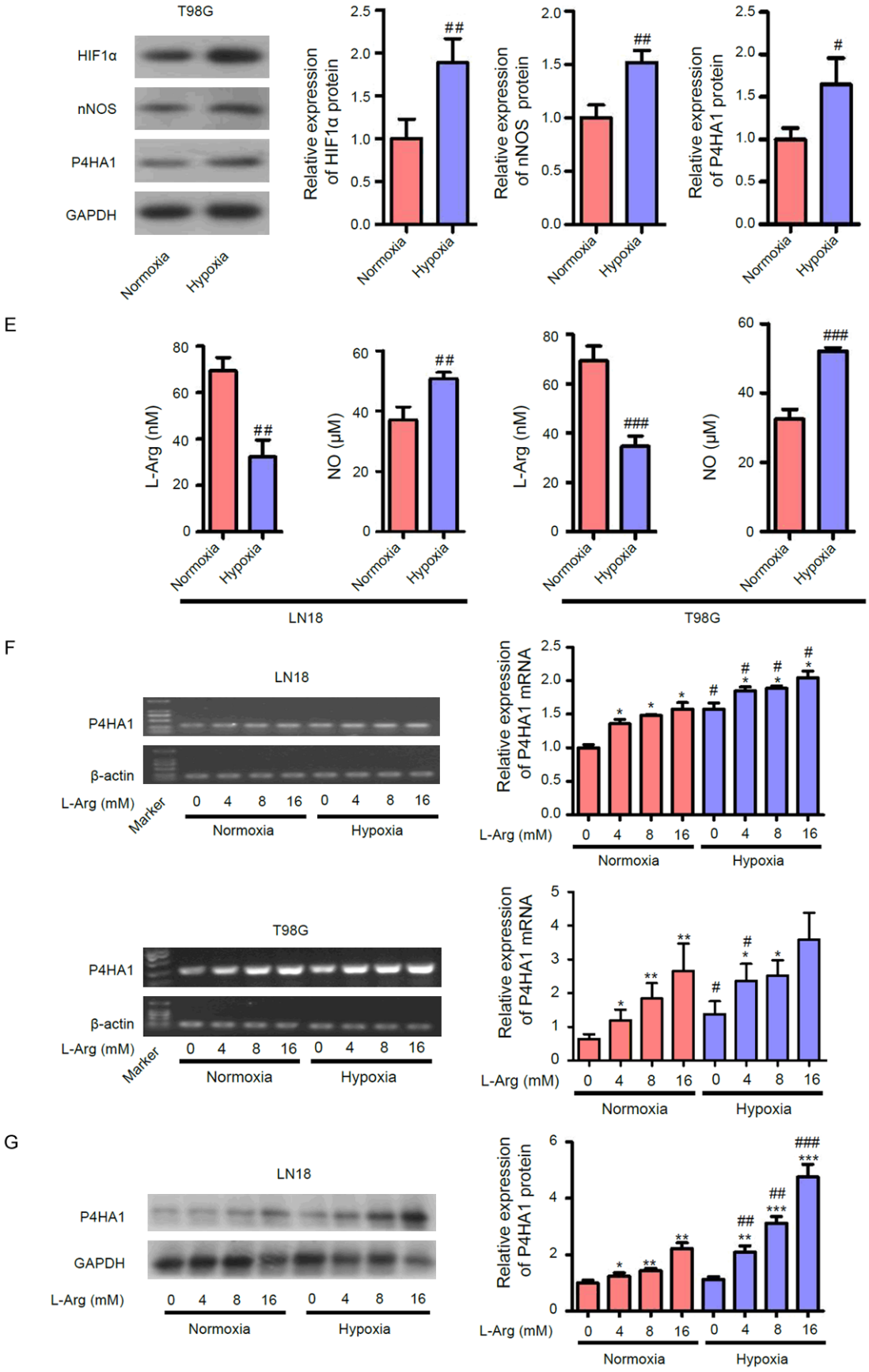
T98G
HIF1α
nNOS
P4HA1
GAPDH
Normoxia
Hypoxia
Relative expression of HIF1α protein
Relative expression of nNOS protein
Relative expression of P4HA1 protein
E
L-Arg (nM)
NO (μM)
LN18
T98G
F
LN18
P4HA1
β-actin
L-Arg (mM)
Marker
0 4 8 16 0 4 8 16
Normoxia
Hypoxia
Relative expression of P4HA1 mRNA
T98G
G
LN18
P4HA1
GAPDH
Relative expression of P4HA1 protein

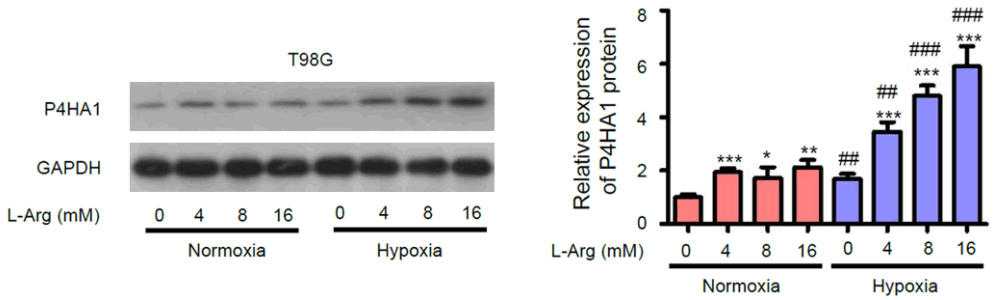

Figure 4. Hypoxia regulates P4HA1 expression and L-Arg production. A, B. Wound-healing and transwell migration assays revealed the migration and invasion activities of LN18 and T98G cells in response to hypoxia. C, D. Levels of the indicated genes and proteins were determined by qRT-PCR and immunoblot assay after culturing the LN18 and T98G cells under normoxia and hypoxia for 24 h. E-G. Quantification of L-Arg and NO concentration in LN18 and T98G cells under both hypoxic and normoxic conditions. Expression of P4HA1 at mRNA and protein levels increased in the presence of external L-Arg in a dose-dependent manner. Results are presented as mean ± SD; n=3; * comparison to siCon and # comparison of hypoxia to normoxia, *** or ###P<0.01, ** or ##0.01<P<0.05, * or #P<0.05, one-way ANOVA test.

oxide (NO) is a critical molecule for signaling transduction in physiological processes, such as tumor progression [34, 35]. Indeed, the NO concentration was increased robustly in response to hypoxia, which lined up well with the elevated nNOS expression and reduced L-Arg concentration (**Figure 4D**).

To elucidate how L-Arg affects P4HA1 expression, we performed immunoblot assays and qRT-PCR using LN18 and T98G cell lines that have been treated with external supply of L-Arg under normoxic and hypoxic conditions. Interestingly, both mRNA and protein levels of P4HA1 showed a continuous increasing pattern in a L-Arg dose-dependent manner. Cells from hypoxic groups all exhibited higher expression of P4HA1 than normoxic groups even with the presence of L-Arg as low as 4 mM (**Figure 4E-G**). Initially, this result seems to be controversial to what we have been reported so far, however, it is good evidence to support that upregulation of P4HA1 promotes glioblastoma invasion via elevated L-Arg catalyzation. Under hypoxia, increased expression of nNOS accelerates the decomposition of excess L-Arg into NO, leading to more hypoxic microenvironment inside the cells, which thus further boost the expression of P4HA1 in response to hypoxia.

HIF1α and nNOS knockdown suppressed P4HA1 expression and invasion of LN18 and T98G cells under hypoxia

To investigate how HIF1α, nNOS and P4HA1 cooperate together under hypoxic environment, we used siRNA to inhibit the expression of HIF1α and then examine the expression of both nNOS and P4HA1 genes. Immunoblot assays and qRT-PCR confirmed the efficient knockdown of HIF1α in cells exposed to normoxia or hypoxia. Depletion of HIF1α resulted in the reduced expression of nNOS and P4HA1 at both mRNA (**Figure 5A**) and protein (**Figure 5B**) levels in LN18 and T98G under hypoxia. Under normoxia, no such change was observed in siHIF1α cells, compared with scrambled controls. As expected, the L-Arg level was significantly increased, while the NO concentration was decreased in siHIF1α cells in hypoxic environment (**Figure 5C**). The concentrations of both L-Arg and NO stayed the same in normoxia in siRNA control groups. To further confirm that HIF1α could influence the expression of nNOS and P4HA1, we also performed the overexpression experiment in both LN18 and T98G cell lines. Interestingly, when HIF1α was overexpressed in both cell lines, neither nNOS or P4HA1 mRNA expression was affected (**Figure 5D**). Consistent with that, the nNOS protein level stays the same with increased HIF1α expression. However, overexpressed HIF1α induce upregulation of P4HA1 protein (**Figure 5E**). Although the difference was not as robust as the knockdown experiments, it is still statistically significant. The inconsistency from HIF1α induction experiment may result from protein overexpression artifacts involving multiple factors. Regardless, actually, it has been shown in fibroblasts that hypoxia-induced P4HA1 expression was mediated by HIF1α. The knockdown of

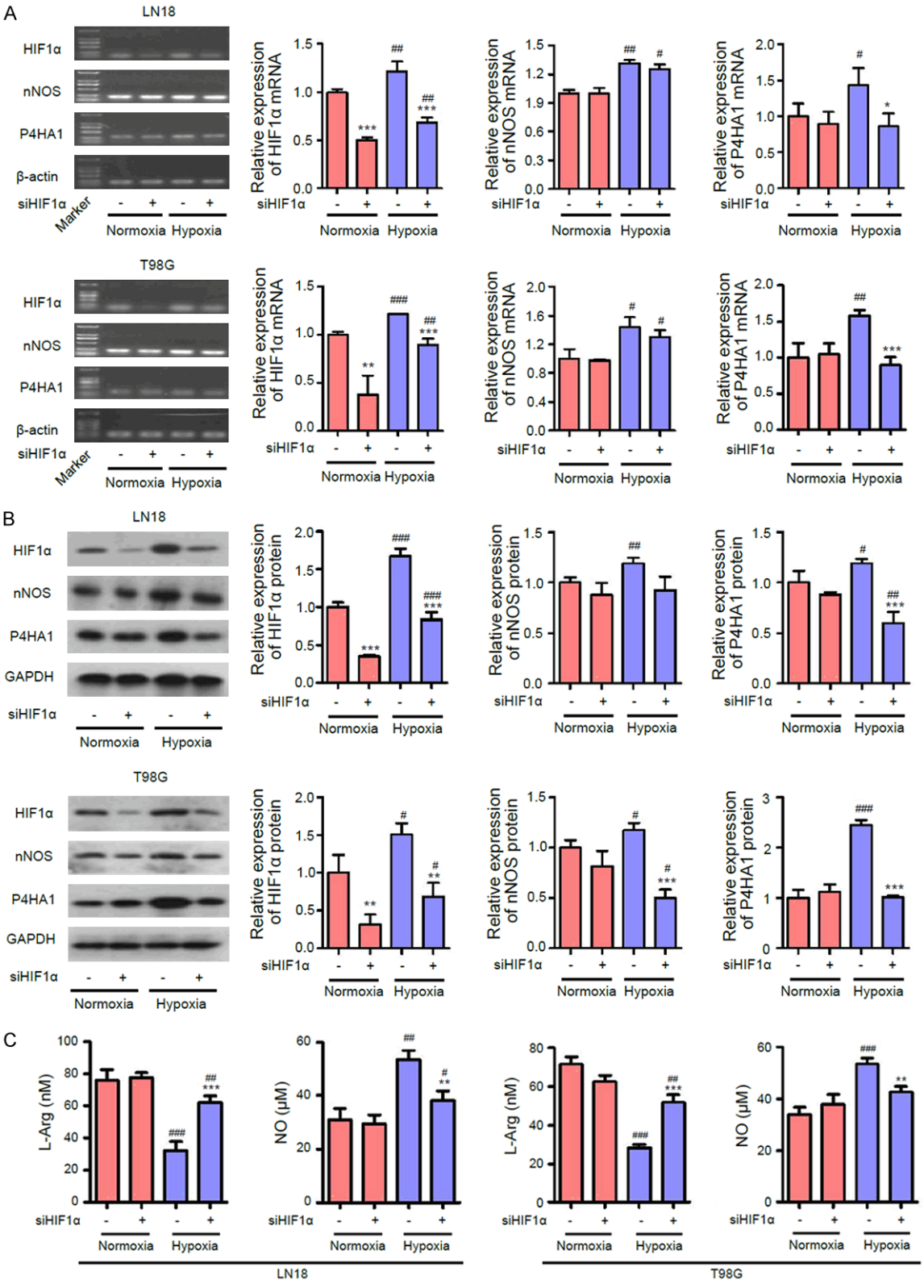
A
LN18
HIF1α
nNOS
P4HA1
β-actin
siHIF1α
Marker
Normoxia
Hypoxia
Relative expression of HIF1α mRNA
Relative expression of nNOS mRNA
Relative expression of P4HA1 mRNA
T98G
B
GAPDH
Relative expression of HIF1α protein
Relative expression of nNOS protein
Relative expression of P4HA1 protein
C
L-Arg (nM)
NO (μM)

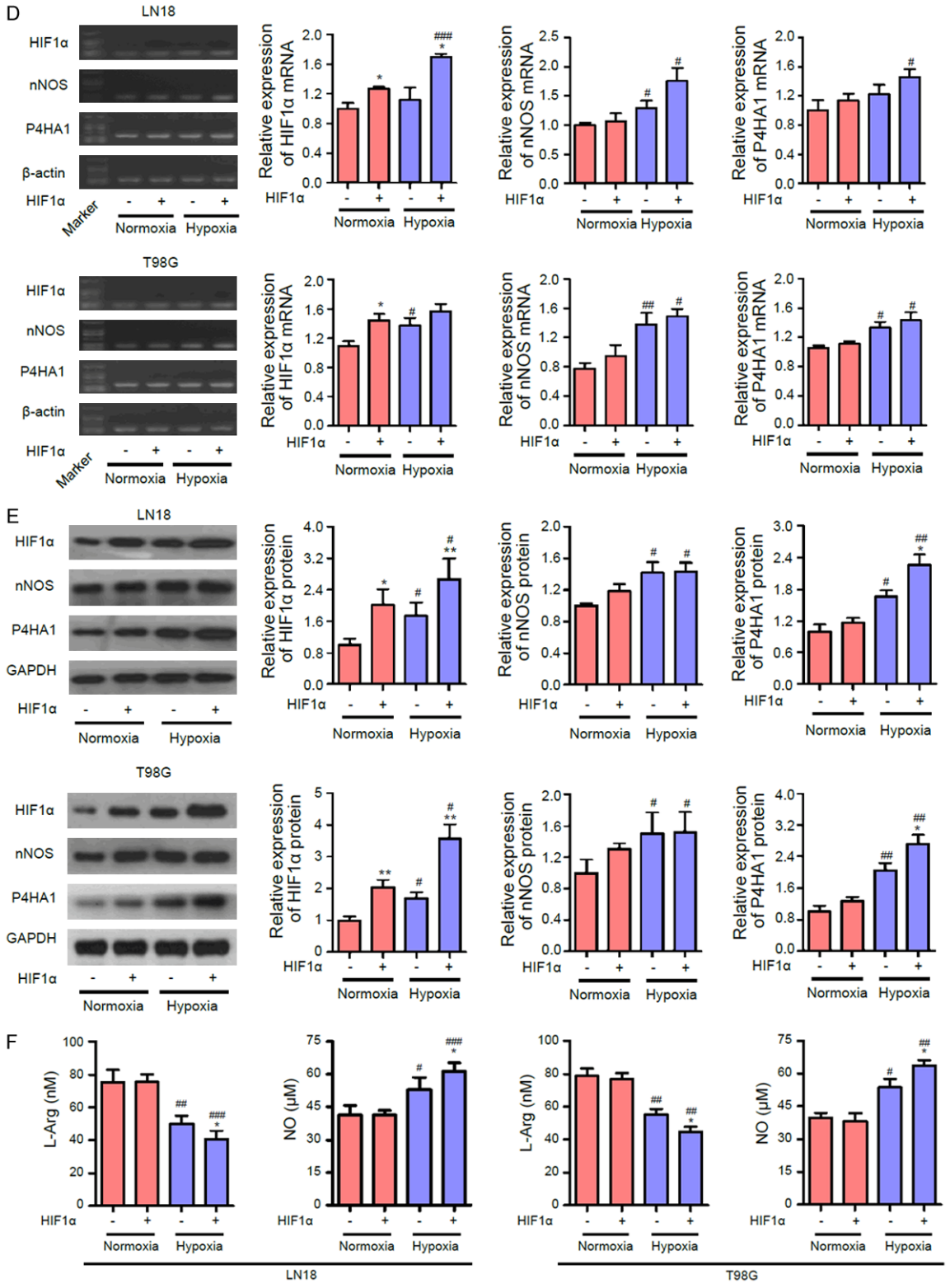

Figure 5. HIF1α enhances the expression of nNOS and P4HA1 and catalyzation of L-Arg. A, B, D and E. Levels of the indicated genes and proteins were determined by qRT-PCR and immunoblot assay after culturing the LN18 and T98G cells under normoxia and hypoxia for 24 h. C. Quantification of L-Arg and NO concentration in siHIF1α LN18 and T98G cells. F. Quantification of L-Arg and NO concentration in HIF1α overexpression LN18 and T98G cells. Results are presented as mean ± SD; n=3; * comparison to siCon and # comparison of hypoxia to normoxia, *** or ###P<0.01, ** or ##0.01<P<0.05, * or #P<0.05, one-way ANOVA test.

HIF-1α abrogated P4HA1 expression from hypoxic induction [28]. Here we found similar regulation mechanism of P4HA1 in glioblastoma. Consistent with the result of siHIF1α cells, the L-Arg level was significantly decreased, while the NO concentration was increased in HIF1α overexpressed cells in hypoxic environment (**Figure 5F**). Taken together, these results suggest that both collagen hydroxylase and nNOS gene expression under hypoxia is HIF1α dependent.

We further studied the expression of P4HA1 when transfecting siRNA of nNOS into LN18 and T98G cells. Similar to the HIF1α, the expressions of nNOS and P4HA1 are positively correlated. Both mRNA and protein levels of P4HA1 decreased under hypoxia in nNOS knockdown cells, while its expression under normoxia remained the same (**Figure 6A** and **6B**). L-Arg concentration almost doubled (from 38 nM to 62 nM in LN18, from 35 nM to 59 nM in T98G) and the NO level decreased significantly in siRNA-nNOS cell cultured under hypoxia (**Figure 6C**). Lastly, to study whether NO concentration influences the expression of P4HA1, we treated the cells with nitric oxide donor (SNP) and assessed the expression of P4HA1 by both qRT-PCR and western blot. We found that the presence of SNP increased the expression of P4HA1 gradually with a dose-dependent manner in both normoxic and hypoxic microenvironment (**Figure 6D** and **6E**). Compared to normoxic group, the expression of P4HA1 was always higher in every single SNP treatment in hypoxic group.

Similar effect was observed in nNOS overexpression cells. The expression level of nNOS was confirmed by both immunoblot assay and RT-PCR. Overexpression of nNOS lead to increased expression of P4HA1 at both mRNA (**Figure 6F**) and protein (**Figure 6G**) levels under hypoxia. No effect was found in normoxic microenvironment at all. As for the metabolic substitute, a significant reduction of L-Arg concentration was revealed in nNOS overexpression cells when cultured in hypoxic condition, while the NO concentration increased dramatically. No such effect was seen under normoxia in the same nNOS overexpression cell lines (**Figure 6H**). Taken together, it implies that hypoxia promotes expression of nNOS through up-regulation of HIF1α, which may stimulate the oxidation of L-Arg to NO; and as an effector molecule, the resulting large amount of NO further activates the expression of P4HA1 in glioblastoma cells.

P4HA1 regulates cell invasion and migration in glioblastoma through molecular switch for EMT program

We have shown that HIF1α and nNOS regulate the expression of P4HA1 in glioblastoma in response to hypoxia. Here we confirmed that P4HA1 is a downstream effector that moderates the hypoxic-induced invasion and migration of glioblastoma by performing both the wound-healing and transwell assays. LN18 and T98G cells had higher migration baseline in response to hypoxia even with reduced expression level of P4HA1. There is slightly decreased migration in siP4HA1 LN18 cells at normal oxygen level compared with siCon cells; however, no difference was observed in T98G cells. Notably, knockdown of P4HA1 significantly impaired the migration in hypoxic LN18 and T98G cells (**Figure 7A**). Depletion of P4HA1 has similar effect on glioblastoma cell invasion. The in vitro assay showed that both siP4HA1 LN18 and T98G cells exhibited decreased invasiveness, fewer cells passed the transwell when P4HA1 was knockdown (**Figure 7B**). Decreased cell invasion was also seen in normoxia, but the effect was much weaker compared with hypoxia. Consistently, both the migration (**Figure 7D**) and invasion (**Figure 7E**) activities of glioblastoma cells were elevated when P4HA1 was overexpressed. The number of both LN28 and T98G cells that invaded the well doubled after 24 h treatment under hypoxia. Because epithelial mesenchymal transition (EMT) has been implicated in cell invasion and tumor progression [36, 37]. And Gilkes et al. discovered that P4HA1 mediated extracellular matrix remodeling under hypoxic conditions to promote carcinoma invasion [28]. We investigated the responses of multiple repressor and activator of EMT while disrupting P4HA1 expression, to understand how P4HA1 modulates glioblastoma migration and invasion under hypoxia. After knockdown of P4HA1, expression of E-cadherin (epithelial marker) increased, while the expression of both Snail, Vimentin, MMP2 and MMP9 (mesenchymal markers) decreased in hypoxic groups, suggesting an inhibition of EMT program (**Figure 7C**). These

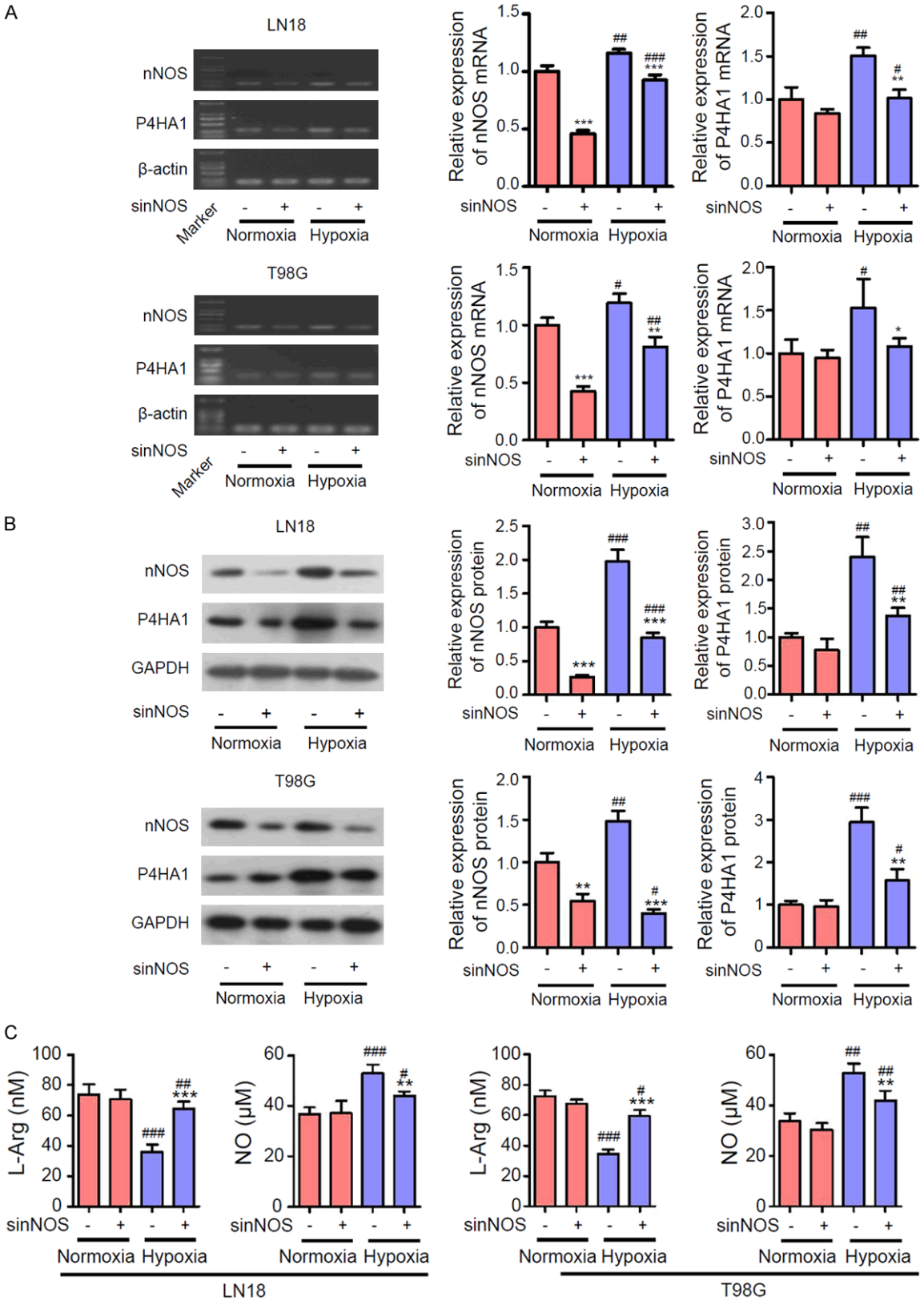
A
LN18
nNOS
P4HA1
β-actin
sinNOS
Marker
Normoxia
Hypoxia
T98G
Relative expression of nNOS mRNA
Relative expression of P4HA1 mRNA
B
GAPDH
Relative expression of nNOS protein
Relative expression of P4HA1 protein
C
L-Arg (nM)
NO (μM)
LN18
T98G

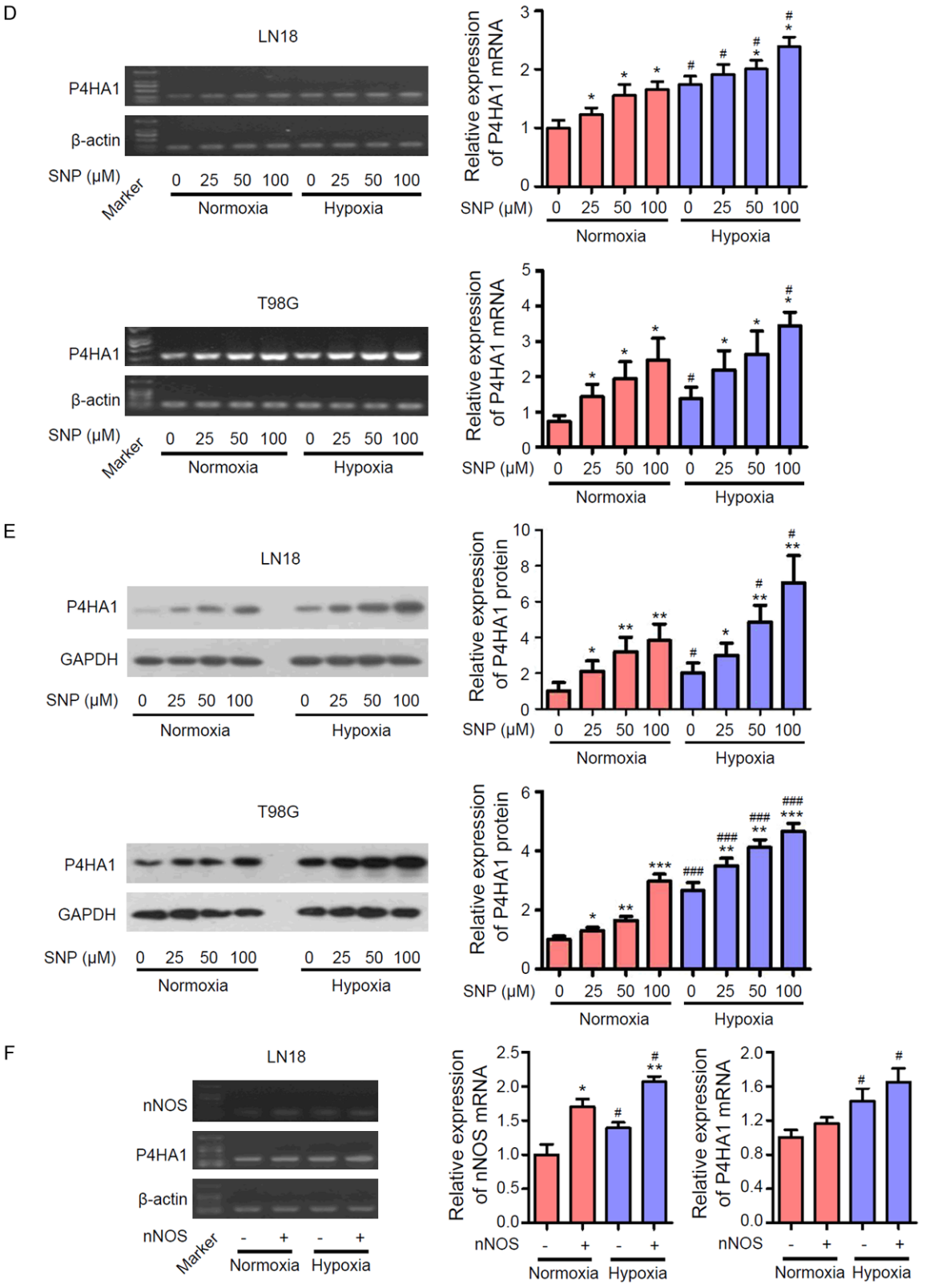
D
LN18
P4HA1
β-actin
SNP (μM)
Marker
0 25 50 100 0 25 50 100
Normoxia
Hypoxia
Relative expression of P4HA1 mRNA
T98G
E
GAPDH
Relative expression of P4HA1 protein
F
nNOS
nNOS
- + - +
Relative expression of nNOS mRNA

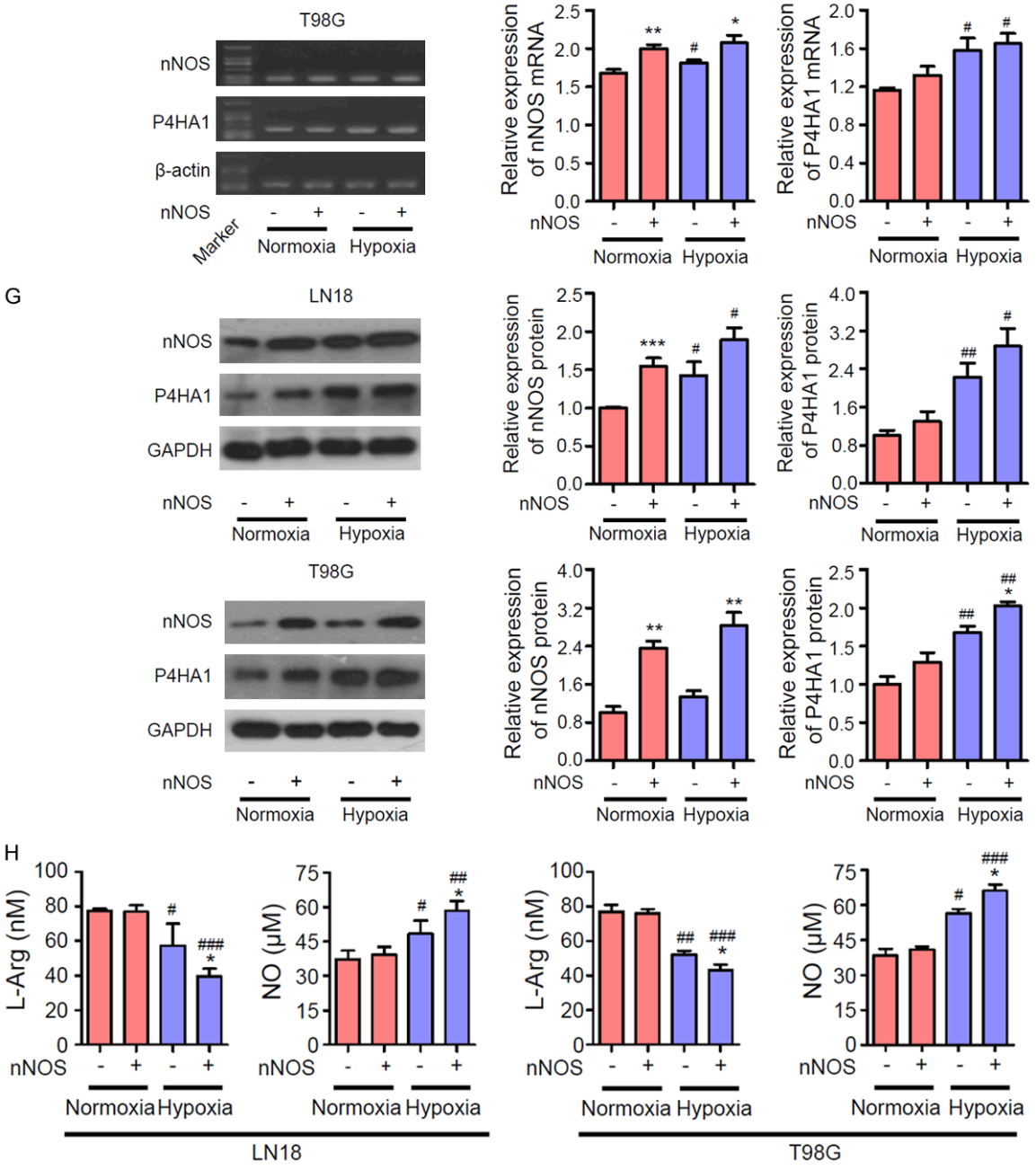

Figure 6. nNOS regulates the expression of P4HA1 and oxidation of L-Arg. A, B, F and G. Expression levels of P4HA1 were determined by qRT-PCR and immunoblot assay after culturing the sinNOS LN18 and T98G cells under normoxia and hypoxia for 24 h. Knockdown efficiency of sinNOS and and overexpression of nNOS was confirmed. C. Quantification of L-Arg and NO concentration in sinNOS LN18 and T98G cells. D, E. Expression of P4HA1 at mRNA and protein levels increased in the presence of SNP in a dose-dependent manner. H. Quantification of L-Arg and NO concentration in nNOS overexpression LN18 and T98G cells. Results are presented as mean ± SD; n=3; * comparison to siCon and # comparison of hypoxia to normoxia, *** or ###P<0.01, ** or ##0.01<P<0.05, * or #P<0.05, one-way ANOVA test.

results were further confirmed by artificially overexpressing P4HA1. When the expression of P4HA1 was boosted, expression of E-cadherin (epithelial marker) decreased, while the expression of both Snail, Vimentin, MMP2 and MMP9 (mesenchymal markers) increased in hypoxic groups (**Figure 7F**). All the results suggest that P4HA1 plays its role in glioblastoma invasion

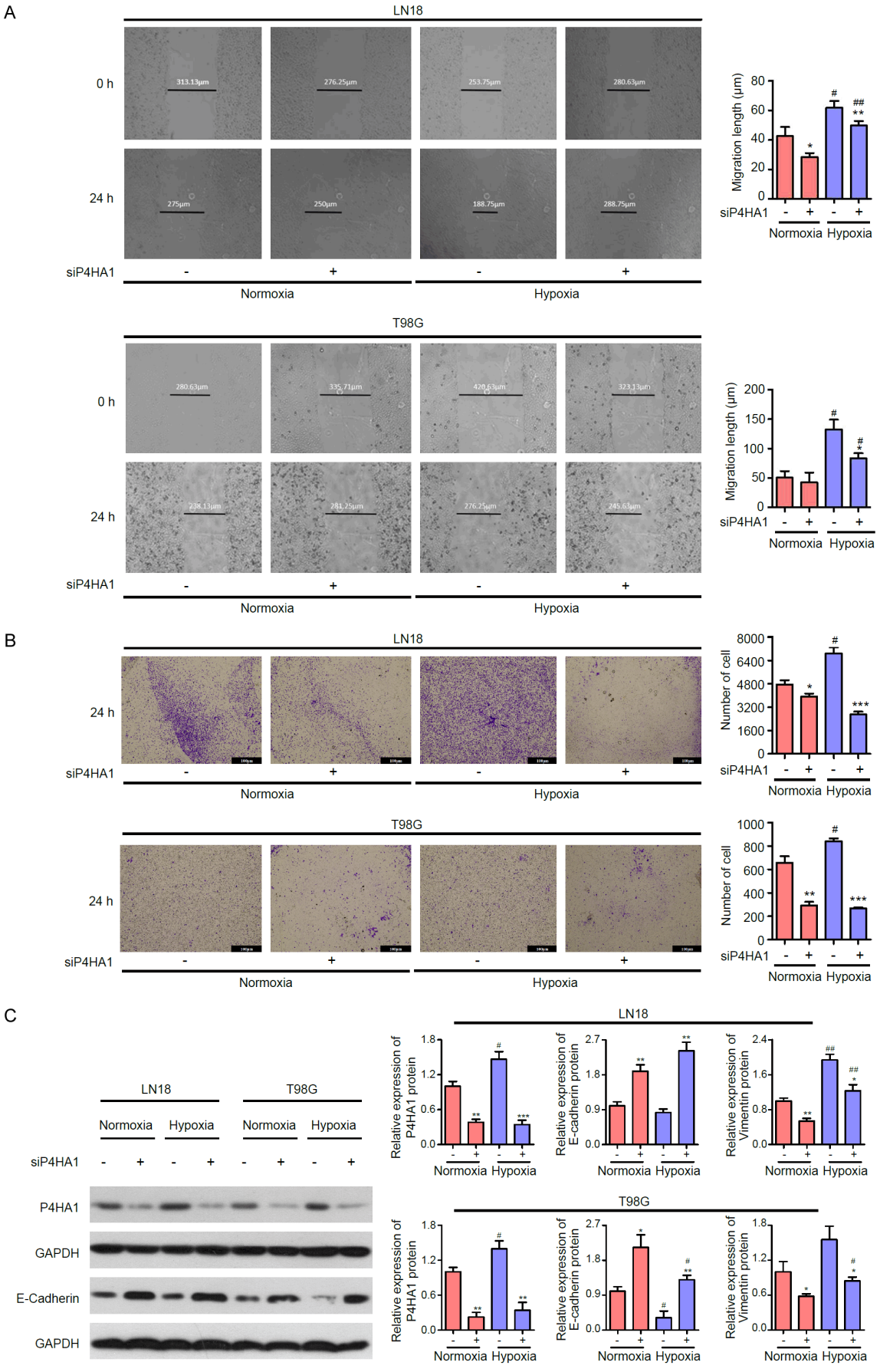
A
LN18
0 h
24 h
313.13μm
276.25μm
253.75μm
280.63μm
275μm
250μm
188.75μm
288.75μm
siP4HA1
Normoxia
Hypoxia
Migration length (μm)
T98G
280.63μm
335.71μm
420.63μm
323.13μm
238.13μm
281.25μm
276.25μm
245.63μm
B
Number of cell
C
LN18
T98G
Normoxia
Hypoxia
siP4HA1
P4HA1
GAPDH
E-Cadherin
GAPDH
Relative expression of P4HA1 protein
Relative expression of E-cadherin protein
Relative expression of Vimentin protein

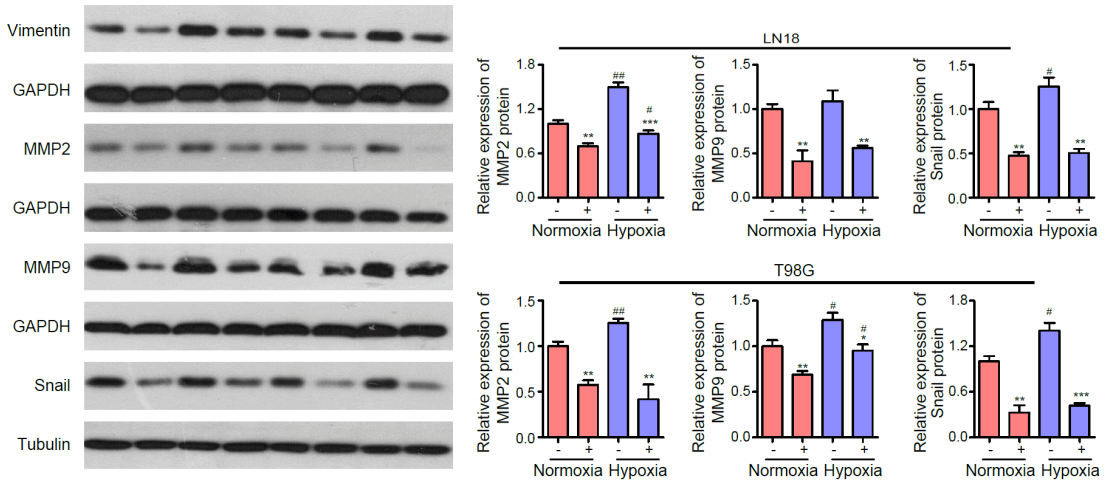
Vimentin
GAPDH
MMP2
GAPDH
MMP9
GAPDH
Snail
Tubulin
LN18
T98G
Relative expression of MMP2 protein
Relative expression of MMP9 protein
Relative expression of Snail protein
Normoxia
Hypoxia

D

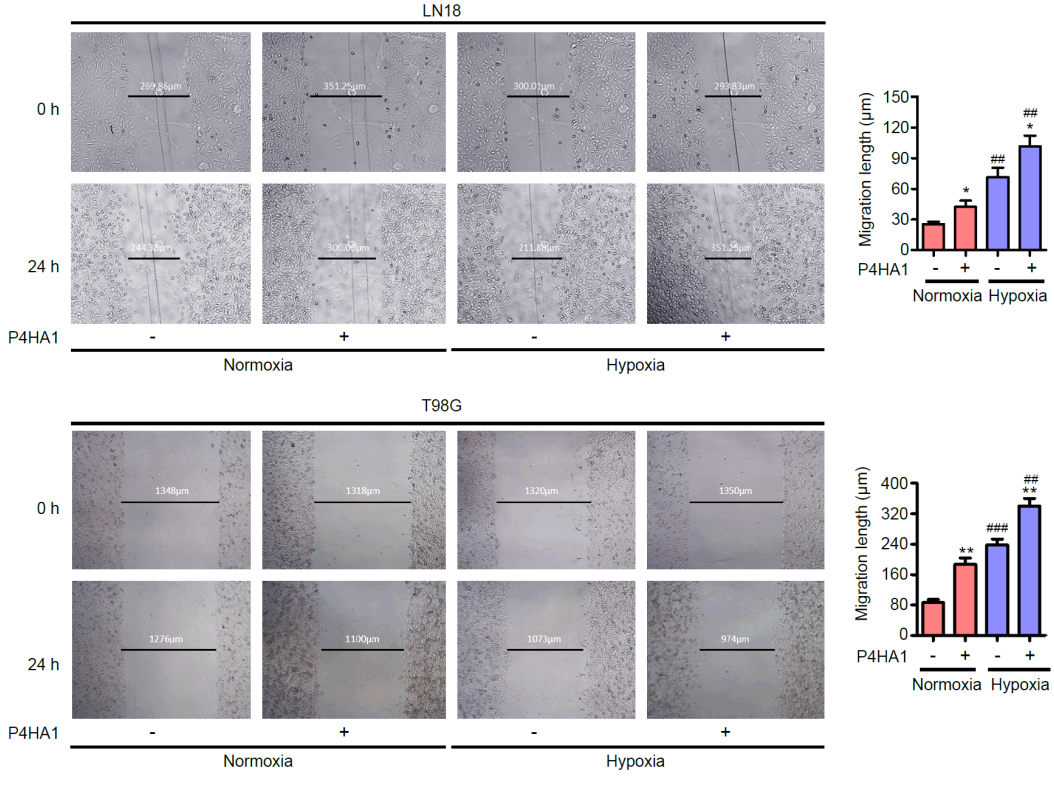
LN18
T98G
0 h
24 h
P4HA1
Normoxia
Hypoxia
Migration length (μm)

E

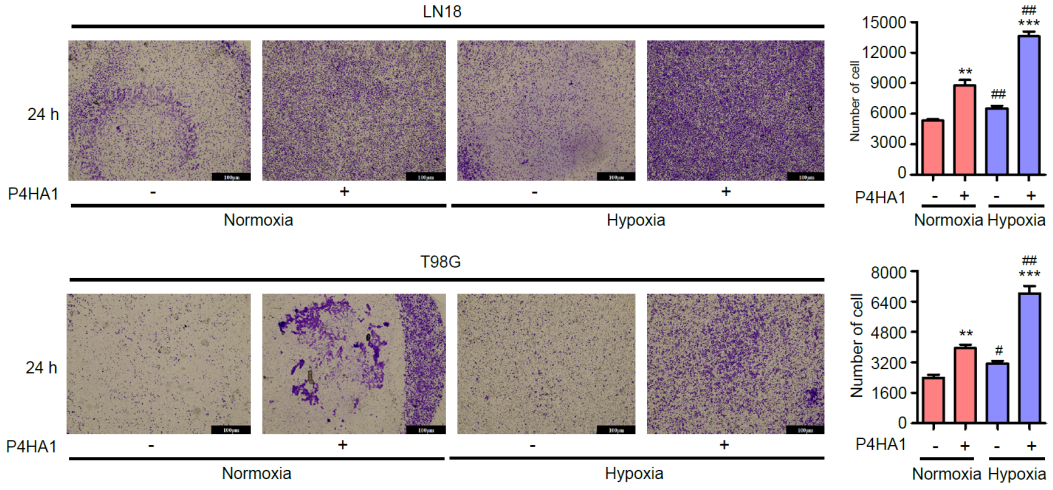
LN18
T98G
24 h
P4HA1
Normoxia
Hypoxia
Number of cell

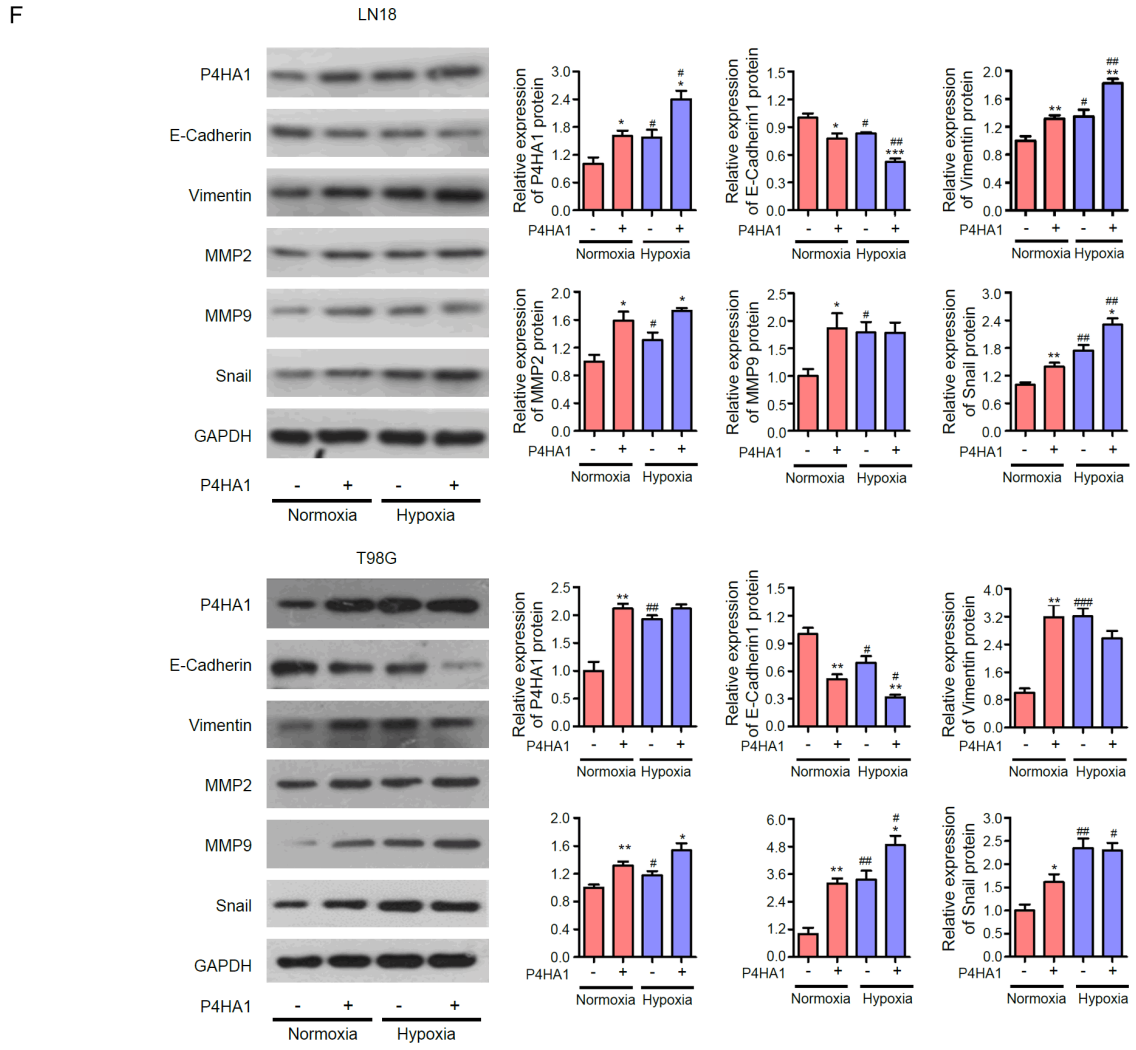

Figure 7. P4HA1 promotes hypoxia-induced glioblastoma migration through remodeling of EMT program. A, D. Wound-healing assays revealed the migration activity in LN18 and T98G cells with disrupted P4HA1 expression. B, E. Transwell migration assays revealed the invasion activity in LN18 and T98G cells with disrupted P4HA1 expression. C, F. Levels of the indicated proteins associated with EMT programing were determined by immunoblot assay after culturing the siP4HA1 or P4HA1 overexpression LN18 and T98G cells under normoxia and hypoxia for 24 h. Results are presented as mean ± SD; n=3; * comparison to siCon and # comparison of hypoxia to normoxia, *** or ###P<0.01, ** or ##0.01<P<0.05, * or #P<0.05, one-way ANOVA test.

via regulating couple effectors in EMT programming.

Expression pattern and prognostic significance of P4HA1 in glioma tissue microarray (TMA), CGGA and TCGA databases

In light of the important functions of P4HA1, we next explored its expression levels in various stages of glioma tissue. The tissue microarray with 128 glioma patients samples were constructed for this purpose. Patients were divided into two groups with low expression (IRS≤7) and high expression (IRS≥8) of P4HA1 in glioma tissue microarray (TMA) was detected by IHC. According to the IRS scores, cytoplasmic expression of P4HA1 was more frequently observed in high-grade gliomas (WHO: III and IV) compared to that in low-grade (WHO: I and II) (**Figure 8A-C**). Analysis of the CGGA and TCGA dataset (including GBM and LGG) showed that high P4HA1 expression was associated with advanced grade glioma (**Figure 8D** and **8E**). Additionally, we evaluated the prognostic

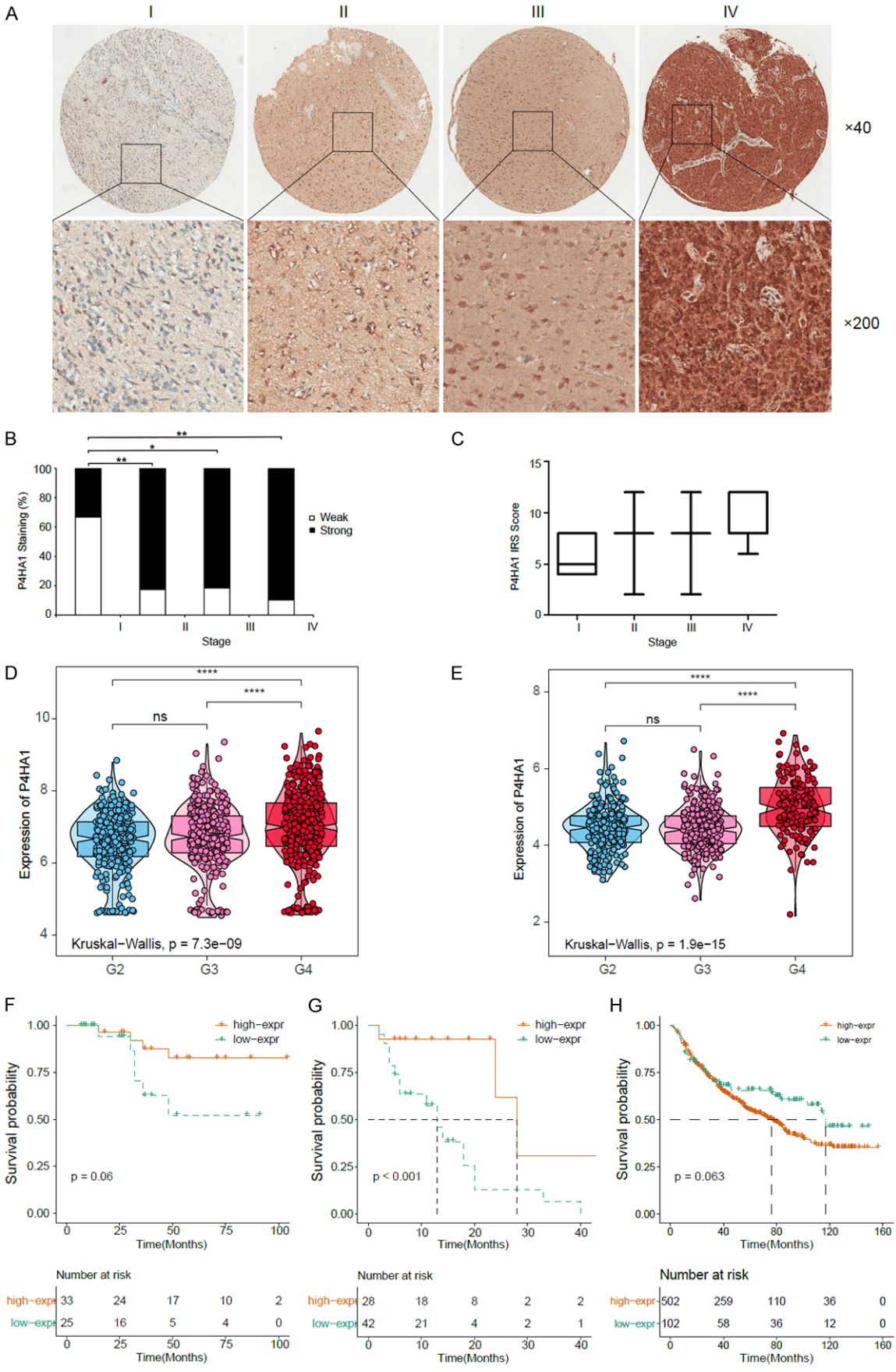
A
I
II
III
IV
×40
×200
B
P4HA1 Staining (%)
Weak
Strong
Stage
C
P4HA1 IRS Score
Stage
D
Expression of P4HA1
ns
Kruskal–Wallis, p = 7.3e−09
G2
G3
G4
E
Expression of P4HA1
ns
Kruskal–Wallis, p = 1.9e−15
G2
G3
G4
F
Survival probability
high−expr
low−expr
p = 0.06
Time(Months)
Number at risk
high−expr 33 24 17 10 2
low−expr 25 16 5 4 0
G
Survival probability
high−expr
low−expr
p < 0.001
Time(Months)
Number at risk
high−expr 28 18 8 2 2
low−expr 42 21 4 2 1
H
Survival probability
high−expr
low−expr
p = 0.063
Time(Months)
Number at risk
high−expr 502 259 110 36 0
low−expr 102 58 36 12 0

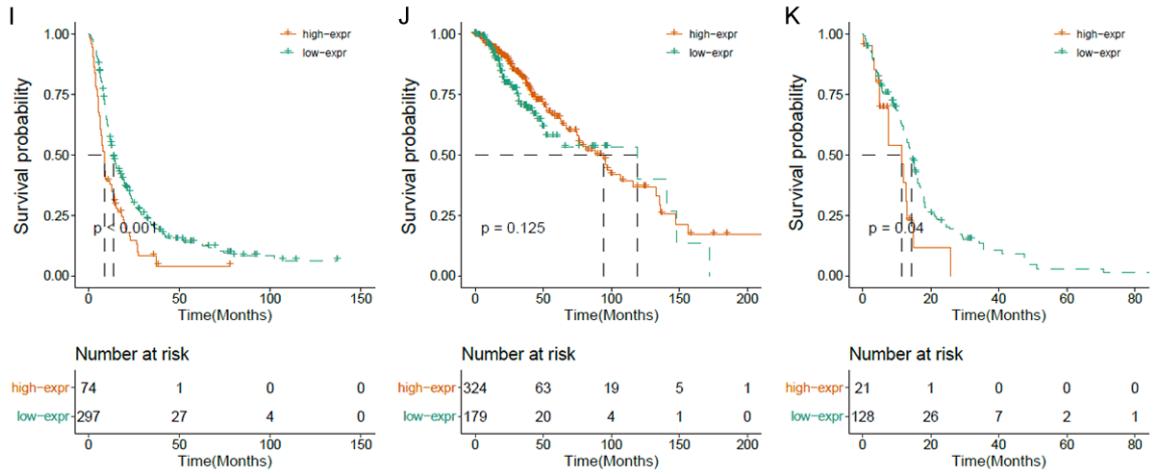

Figure 8. Analysis of P4HA1 expression and survival in glioblastoma patients from tissue microarray (TMA), CGGA and TCGA database. A. Immunohistochemical staining of P4HA1 in different WHO grades glioma tissues. B. Increased cytoplasmic P4HA1 expression correlates with subtype glioma. C. Data from TMA revealed that P4HA1 expression increased in grade II, III and IV glioma compared with that in grade I. D, E. P4HA1 expression pattern in different subtypes in CGGA and TCGA data set. F, G. Increased P4HA1 expression correlated with poor prognosis for high-grade gliomas but not low-grade ones. H, I. Data from the CGGA showed that increased P4HA1 expression correlated with poor prognosis for high-grade gliomas but not low-grade ones. J, K. TCGA analysis showed that high expression of P4HA1 conferred a worse prognosis in high-grade glioma patients than that in low-grade ones. ***P<0.01, **0.01<P<0.05, *P<0.05, with one-way ANOVA.

capacity of P4HA1 expression in different grades of glioma patients. We demonstrated that high P4HA1 expression correlated significantly with shorter OS in the high-grade gliomas (WHO: III and IV) (**Figure 8G**) but not in that with low-grade gliomas (WHO: I and II) (**Figure 8F**). In support of above conclusions, we used CGGA combined with TCGA databases to analyze the impact of P4HA1 on survival probability in high and low grade gliomas. The results indicated that P4HA1 expression correlated with survival probability in high grade subgroup (**Figure 8I** and **8K**), while low grade subgroup had no such correlation (**Figure 8H** and **8J**). Our data demonstrated that P4HA1 was upregulated in high-grade gliomas compared to low grade ones. Overexpression of P4HA1 was independently correlated with the decreased survival for patients with high-grade gliomas. Hu et al. found that P4HA1 was upregulated in gliomas and high expression of P4HA1 was correlated with the malignancy of gliomas and could serve as a prognostic indicator for patients with high-grade gliomas [38]. Our result was consistent with Hu's research.

Discussion

Glioblastoma multiforme is the most common primary brain tumor in adults, accounting for about 50-70% of the primary tumors of the central nervous system. The invasive growth of the tumors leads to poor prognosis despite the combination of surgery, radiotherapy and chemotherapy. Therefore, an in-depth understanding of the malignant behavior of glioblastoma and the underlying molecular mechanism is a key research to seek efficient treatment of glioma. Previous studies have found that hypoxia could accelerate the infiltration and growth of glioblastoma, however, the molecular mechanism remains obscure. In this study, we performed metabolomic and proteomic profiling in LN18 cell line to identify the key metabolites and proteins in hypoxia-induced cell invasion. In summary, we found 1,160 and 1,958 significant differential anions and cations, which are mainly enriched in the metabolic processes such as the tricarboxylic acid cycle, lipid metabolism, glycolysis, amino acid and nucleic acid metabolic pathway. The proteomic analysis identified 62 significantly differentially expressed proteins, of which 28 were up-regulated and 34 were down-regulated. Additional integration analysis (including comparative and correlation analysis, GO function analysis, metabolic pathway enrichment) revealed that among the significantly differential molecules, 7 proteins and 10 metabolites are strongly cor-

related. We further characterized the function of one pair (L-Arg and P4HA1) of particular interest.

L-Arg is involved in several metabolic pathways. It is not only a basic building unit of protein, but also a precursor for the synthesis of urea, polyamines, proline, glutamic acid, creatine and agmatine [39]. L-Arg has been shown closely related to carcinogenesis, tumor suppression and biological behavior of tumor through various biological metabolic pathways [40]. L-Arg is decomposed by NOS to produce NO and citrulline, thereby promoting the occurrence and development of malignant tumors. The cationic amino acid transport system can also selectively accumulate arginine directly on the plasma membrane to synthesize NO. Although it has been reported that L-Arg can inhibit the process of carcinogenesis, such as colorectal adenoma to adenocarcinoma [41], whether L-Arg affects the invasiveness of glioblastoma is unclear. 4-Hydroxy-prolyl hydroxylase (P4H) is a key enzyme in collagen synthesis, which is a tetramer composed of two alpha subunits and two beta subunits. P4H can catalyze the formation of hydroxyproline by hydroxylating the proline residue on the X-Pro-Gly sequence, which facilitates the formation of a stable two-helix molecular structure of the collagen polypeptide chain [42, 43]. P4HA1 is an isozyme of P4H. Several studies have found that regulating the expression of P4HA1 can affect the stability of atherosclerotic plaque [44] and it also promotes tumor cell infiltration [45]. So far no study is available on the relationship between L-Arg and P4HA1 in the invasiveness of glioblastoma in hypoxia.

Our integrative analysis first revealed that L-Arg and P4HA1 were strongly anti-correlated, that is, the concentration of L-Arg decreased while the expression of P4HA1 increased after hypoxia treatment. The following functional analysis showed that along with P4HA1, the expression of HIF1α, nNOS also increased after hypoxia treatment in glioblastoma cell lines LN18 and T98G. HIF1α has been confirmed as a key transcription factor that mediates hypoxia signaling, which is activated by binding to hypoxic response elements (HREs) [46]. Its downstream targets are involved in tumor proliferation and invasion, energy metabolism, and chemoradiation resistance [47]. One target family of HIF1α are NOSs [48]. HIF1α regulates type II NOS gene expression in response to hypoxia in pulmonary artery endothelial cells [49]. Over-expression of iNOS is implicated in tumor angiogenesis in human colorectal carcinoma [50]. We found that the expression of nNOS and P4HA1 decreased after HIF1α interference. As expected, the L-Arg concentration was increased while NO concentration was decreased. Overexpression of HIF1α did not increase the expression of nNOS and P4HA1 as expected, which was a bit surprising. We think this result may cause by artificial effect of overexpression, such as unphysiologically protein concentrations. A titration of overexpression or change of an inducible promoter may provide more information on that. Knockdown of nNOS impaired the expression of P4HA1, while overexpression of nNOS increase the expression of this protein. We also observed increased NO concentration after NO donor sodium nitroprusside (SNP) treatment enhanced the expression of P4HA1, suggesting NO as a potential messager to regulate P4HA1 expression. How NO regulates P4HA1 is beyond the scope of the current work and we will study it in the future.

To understand how P4HA1 promotes glioblastoma invasion, we examined the expression of genes involved in epithelial mesenchymal transition pathway. EMT is considered to be the initial link of solid tumor metastasis and has received much attention in recent years [36]. Studies have shown that the regulation of HIF1α expression in cells can affect the occurrence of EMT. Krishnamachary et al. found that hypoxia or gene transfection overexpression of HIF1α increased the expression of Vimentin in colon cancer cell line HCT116 and its invasive ability in vitro, and interference with HIF-1α expression reversed this phenomenon [51]. Luo et al. transfected the recombinant plasmid pc DNA3.1(-)/HIF-1α into the prostate cancer cell line LNCaP to overexpress HIF-1α, which increased the expression of Vimentin and decreased the expression of E-cadherin [52]. In our study, we found that depletion of P4HA1 resulted in reduced LN18 and T98G cell migration, associated with down-regulation of Snail, MMP2, MMP9 and Vimentin, and up-regulation of E-cadherin. Overexpression of P4HA1 reverses these effects on the EMT genes.

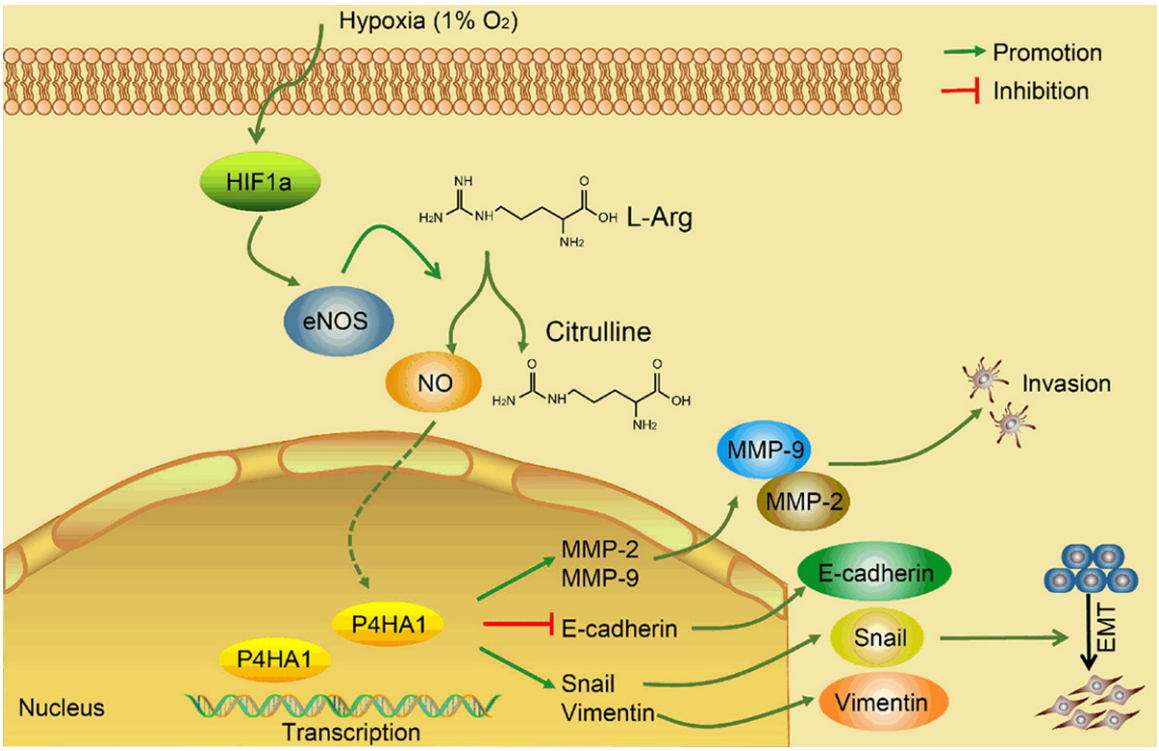

Figure 9. Schematic representation of downstream signaling cascade associated with hypoxia-initiated cell invasion of glioblastoma.

Taken together, we propose a simple model of how P4HA1 induce glioblastoma invasion in response to hypoxia (**Figure 9**). 1) Hypoxia enhances the expression of HIF1α; 2) Which further up-regulates nNOS expression; 3) While nNOS is the rate-limiting enzyme of L-Arg catabolism, it promotes L-Arg decomposition, resulting in excess amount of NO and citrulline; 4) NO is a signal transduction molecule, that activate the expression of P4HA1; 5) Activation of P4HA1 promotes the expression of MMP2, MMP9, Snail and Vimentin, inhibits the expression of E-cadherin; 6) The reprogramming of EMT leads to the increased invasiveness of glioma cells.

Traditionally, the study of how hypoxia affects glioblastoma progression and metastasis mainly focused on individual genes. Recently researchers started to understand the global molecular networking under the pathological process through multi-omics analysis. However, these works are limited to investigating the interaction of biological macromolecules such as proteins and DNA. Little is known about how these macromolecules and metabolites function together. Here we take advantage of both metabolic and proteomic profiling to identify key regulators in glioblastoma invasion under hypoxia conditions, which is a great resource of understanding glioblastoma pathology. Expression pattern and prognostic significance of P4HA1 in gliomas tissues specimens remains unknown. Quite recently, Hu et al. has demonstrated that expression of P4HA1 was correlated with advanced histological grade and significantly associated with poor prognosis for high-grade gliomas, which as an independent risk factor for prognosis [38]. Our data, combined with Hu's findings, suggest the important role of P4HA1 in glioma progression, and made P4HA1 a promising target against gliomas. Moreover, we depict a novel pathway that regulates the invasiveness of glioma cells. Lastly, the discovery of how L-Arg affects the EMT mediated GBM cell invasion suggests a new strategy for therapy by targeting tumor metabolism.

Acknowledgements

Thanks to Beijing Protein Innovation Co., Ltd. for the metabolomics (LC-MS), proteomics (Label Free) and MRM analysis. We also thank

the Shanghai Luming Biological Technology Co., LTD. (Shanghai, China) for providing proteomics and metabolomics correlation analysis services. This work was supported by the major research plan of the National Natural Science Foundation of China (91959125 and 81972336), Shanghai Municipal Science and Technology Major Project (19410740300) and the Xiamen Health Science and Technology Program (3502Z20194050 and 3502Z2018-4067).

Disclosure of conflict of interest

None.

Address correspondence to: Dr. Tianhai Ji, Department of Pathology, Ninth People's Hospital, Shanghai Jiaotong University School of Medicine, Shanghai 200011, China. Tel: 86-21-53315212; Fax: 86-21-53315212; E-mail: skysea_ji@sina.com

References

[1] Thakkar JP, Dolecek TA, Horbinski C, Ostrom QT, Lightner DD, Barnholtz-Sloan JS and Villano JL. Epidemiologic and molecular prognostic review of glioblastoma. Cancer Epidemiol Biomarkers Prev 2014; 23: 1985-1996.

[2] Wright CH, Wright J, Onyewadume L, Raghavan A, Lapite I, Casco-Zuleta A, Lagman C, Sajatovic M and Hodges TR. Diagnosis, treatment, and survival in spinal dissemination of primary intracranial glioblastoma: systematic literature review. J Neurosurg Spine 2019; 1-10.

[3] Field KM, Jordan JT, Wen PY, Rosenthal MA and Reardon DA. Bevacizumab and glioblastoma: scientific review, newly reported updates, and ongoing controversies. Cancer 2015; 121: 997-1007.

[4] Ramezani S, Vousooghi N, Joghataei MT and Chabok SY. The role of kinase signaling in resistance to bevacizumab therapy for glioblastoma multiforme. Cancer Biother Radiopharm 2019; 34: 345-354.

[5] Colwell N, Larion M, Giles AJ, Seldomridge AN, Sizdahkhani S, Gilbert MR and Park DM. Hypoxia in the glioblastoma microenvironment: shaping the phenotype of cancer stem-like cells. Neuro Oncol 2017; 19: 887-896.

[6] Papale M, Buccarelli M, Mollinari C, Russo MA, Pallini R, Ricci-Vitiani L and Tafani M. Hypoxia, inflammation and necrosis as determinants of glioblastoma cancer stem cells progression. Int J Mol Sci 2020; 21: 2660.

[7] Chen JE, Lumibao J, Blazek A, Gaskins HR and Harley B. Hypoxia activates enhanced invasive potential and endogenous hyaluronic acid production by glioblastoma cells. Biomater Sci 2018; 6: 854-862.

[8] Gagner JP, Lechpammer M and Zagzag D. Induction and assessment of hypoxia in glioblastoma cells in vitro. Methods Mol Biol 2018; 1741: 111-123.

[9] Huang W, Ding X, Ye H, Wang J, Shao J and Huang T. Hypoxia enhances the migration and invasion of human glioblastoma U87 cells through PI3K/Akt/mTOR/HIF-1α pathway. Neuroreport 2018; 29: 1578-1585.

[10] Curtin L, Hawkins-Daarud A, van der Zee KG, Swanson KR and Owen MR. Speed switch in glioblastoma growth rate due to enhanced hypoxia-induced migration. Bull Math Biol 2020; 82: 43.

[11] Łuczak MW, Roszak A, Pawlik P, Kędzia H, Lianeri M and Jagodziński PP. Increased expression of HIF-1A and its implication in the hypoxia pathway in primary advanced uterine cervical carcinoma. Oncol Rep 2011; 26: 1259-1264.

[12] Wang Y, Liu Z, Lian B, Liu L and Xie L. Integrative analysis of dysfunctional modules driven by genomic alterations at system level across 11 cancer types. Comb Chem High Throughput Screen 2018; 21: 771-783.

[13] Zhou B and Guo R. Integrative analysis of significant RNA-binding proteins in colorectal cancer metastasis. J Cell Biochem 2018; 119: 9730-9741.

[14] Wei R, De Vivo I, Huang S, Zhu X, Risch H, Moore JH, Yu H and Garmire LX. Meta-dimensional data integration identifies critical pathways for susceptibility, tumorigenesis and progression of endometrial cancer. Oncotarget 2016; 7: 55249-55263.

[15] Shaw PG, Chaerkady R, Wang T, Vasilatos S, Huang Y, Van Houten B, Pandey A and Davidson NE. Integrated proteomic and metabolic analysis of breast cancer progression. PLoS One 2013; 8: e76220.

[16] Kodama M, Oshikawa K, Shimizu H, Yoshioka S, Takahashi M, Izumi Y, Bamba T, Tateishi C, Tomonaga T, Matsumoto M and Nakayama KI. A shift in glutamine nitrogen metabolism contributes to the malignant progression of cancer. Nat Commun 2020; 11: 1320.

[17] Zhang Y, Nguyen TTT, Shang E, Mela A, Humala N, Mahajan A, Zhao J, Shu C, Torrini C, Sanchez-Quintero MJ, Kleiner G, Bianchetti E, Westhoff MA, Quinzii CM, Karpel-Massler G, Bruce JN, Canoll P and Siegelin MD. MET inhibition elicits PGC1α-dependent metabolic reprogramming in glioblastoma. Cancer Res 2020; 80: 30-43.

[18] Wang Y, Li Y, Cang S, Cai Q, Xu H, Wang Y, Liu R, Xu H and Li Q. Qualitative and quantitative analysis of pyrrolizidine alkaloids for the entire

process quality control from Senecio scandens to Senecio scandens-containing preparations by high performance liquid chromatography-tandem mass spectrometry. J Mass Spectrom 2020; 55: e4532.
[19] Chen X, Liu X, Deng B, Martinka M, Zhou Y, Lan X and Cheng Y. Cytoplasmic Pin1 expression is increased in human cutaneous melanoma and predicts poor prognosis. Sci Rep 2018; 8: 16867.
[20] Li P, Zhou C, Xu L and Xiao H. Hypoxia enhances stemness of cancer stem cells in glioblastoma: an in vitro study. Int J Med Sci 2013; 10: 399-407.
[21] Gao Y, Zhang E, Liu B, Zhou K, He S, Feng L, Wu G, Cao M, Wu H, Cui Y, Zhang X, Liu X, Wang Y, Gao Y and Bian X. Integrated analysis identified core signal pathways and hypoxic characteristics of human glioblastoma. J Cell Mol Med 2019; 23: 6228-6237.
[22] Armitage EG, Kotze HL, Allwood JW, Dunn WB, Goodacre R and Williams KJ. Metabolic profiling reveals potential metabolic markers associated with hypoxia Inducible factor-mediated signalling in hypoxic cancer cells. Sci Rep 2015; 5: 15649.
[23] González-Pacheco H, Méndez-Domínguez A, Hernández S, López-Marure R, Vazquez-Mellado MJ, Aguilar C and Rocha-Zavaleta L. Preconditioning with CDP-choline attenuates oxidative stress-induced cardiac myocyte death in a hypoxia/reperfusion model. ScientificWorldJournal 2014; 2014: 187071.
[24] Jang JH, Baerts L, Waumans Y, De Meester I, Yamada Y, Limani P, Gil-Bazo I, Weder W and Jungraithmayr W. Suppression of lung metastases by the CD26/DPP4 inhibitor Vildagliptin in mice. Clin Exp Metastasis 2015; 32: 677-687.
[25] Huang L, Zhou Y, Cao XP, Lin JX, Zhang L, Huang ST and Zheng M. KPNA2 promotes migration and invasion in epithelial ovarian cancer cells by inducing epithelial-mesenchymal transition via Akt/GSK-3β/Snail activation. J Cancer 2018; 9: 157-165.
[26] Zhang M, Li ZF, Wang HF, Wang SS, Yu XH, Wu JB, Pang X, Wu JS, Yang X, Tang YJ, Li L, Liang XH, Zheng M and Tang YL. MIF promotes perineural invasion through EMT in salivary adenoid cystic carcinoma. Mol Carcinog 2019; 58: 898-912.
[27] Peng M, Yang D, Hou Y, Liu S, Zhao M, Qin Y, Chen R, Teng Y and Liu M. Intracellular citrate accumulation by oxidized ATM-mediated metabolism reprogramming via PFKP and CS enhances hypoxic breast cancer cell invasion and metastasis. Cell Death Dis 2019; 10: 228.
[28] Gilkes DM, Bajpai S, Chaturvedi P, Wirtz D and Semenza GL. Hypoxia-inducible factor 1 (HIF-1) promotes extracellular matrix remodeling under hypoxic conditions by inducing P4HA1, P4HA2, and PLOD2 expression in fibroblasts. J Biol Chem 2013; 288: 10819-10829.
[29] Okumura Y and Eguchi H. ASO author reflections: hypoxia-induced PLOD2 is a key regulator in epithelial-mesenchymal transition and chemoresistance in biliary tract cancer. Ann Surg Oncol 2018; 25: 3738-3739.
[30] Horiuchi A, Hayashi T, Kikuchi N, Hayashi A, Fuseya C, Shiozawa T and Konishi I. Hypoxia upregulates ovarian cancer invasiveness via the binding of HIF-1α to a hypoxia-induced, methylation-free hypoxia response element of S100A4 gene. Int J Cancer 2012; 131: 1755-1767.
[31] Kaur B, Khwaja FW, Severson EA, Matheny SL, Brat DJ and Van Meir EG. Hypoxia and the hypoxia-inducible-factor pathway in glioma growth and angiogenesis. Neuro Oncol 2005; 7: 134-153.
[32] Semenza GL. Molecular mechanisms mediating metastasis of hypoxic breast cancer cells. Trends Mol Med 2012; 18: 534-543.
[33] Li G, Zhao Y, Li Y and Lu J. Up-regulation of neuronal nitric oxide synthase expression by cobalt chloride through a HIF-1α mechanism in neuroblastoma cells. Neuromolecular Med 2015; 17: 443-453.
[34] Lala PK and Orucevic A. Role of nitric oxide in tumor progression: lessons from experimental tumors. Cancer Metastasis Rev 1998; 17: 91-106.
[35] Wiesinger H. Arginine metabolism and the synthesis of nitric oxide in the nervous system. Prog Neurobiol 2001; 64: 365-391.
[36] Pastushenko I and Blanpain C. EMT transition states during tumor progression and metastasis. Trends Cell Biol 2019; 29: 212-226.
[37] Lah TT, Novak M and Breznik B. Brain malignancies: glioblastoma and brain metastases. Semin Cancer Biol 2020; 60: 262-273.
[38] Hu WM, Zhang J, Sun SX, Xi SY, Chen ZJ, Jiang XB, Lin FH, Chen ZH, Chen YS, Wang J, Yang QY, Guo CC, Mou YG, Chen ZP, Zeng J and Sai K. Identification of P4HA1 as a prognostic biomarker for high-grade gliomas. Pathol Res Pract 2017; 213: 1365-1369.
[39] Wu G and Morris SM Jr. Arginine metabolism: nitric oxide and beyond. Biochem J 1998; 336: 1-17.
[40] Szende B, Tyihák E and Trézl L. Role of arginine and its methylated derivatives in cancer biology and treatment. Cancer Cell Int 2001; 1: 3.
[41] Ma Q, Wang Y, Gao X, Ma Z and Song Z. L-arginine reduces cell proliferation and ornithine decarboxylase activity in patients with colorectal adenoma and adenocarcinoma. Clin Cancer Res 2007; 13: 7407-7412.

[42] Murthy AV, Sulu R, Koski MK, Tu H, Anantharajan J, Sah-Teli SK, Myllyharju J and Wierenga RK. Structural enzymology binding studies of the peptide-substrate-binding domain of human collagen prolyl 4-hydroxylase (type-II): high affinity peptides have a PxGP sequence motif. Protein Sci 2018; 27: 1692-1703.
[43] D'Aniello C, Patriarca EJ, Phang JM and Minchiotti G. Proline metabolism in tumor growth and metastatic progression. Front Oncol 2020; 10: 776.
[44] Cao XQ, Liu XX, Li MM, Zhang Y, Chen L, Wang L, Di MX and Zhang M. Overexpression of Prolyl-4-hydroxylase-α1 stabilizes but increases shear stress-induced atherosclerotic plaque in apolipoprotein E-deficient mice. Dis Markers 2016; 2016: 1701637.
[45] Gilkes DM, Chaturvedi P, Bajpai S, Wong CC, Wei H, Pitcairn S, Hubbi ME, Wirtz D and Semenza GL. Collagen prolyl hydroxylases are essential for breast cancer metastasis. Cancer Res 2013; 73: 3285-3296.
[46] Bruick RK. Oxygen sensing in the hypoxic response pathway: regulation of the hypoxia-inducible transcription factor. Genes Dev 2003; 17: 2614-2623.
[47] Goda N, Dozier SJ and Johnson RS. HIF-1 in cell cycle regulation, apoptosis, and tumor progression. Antioxid Redox Signal 2003; 5: 467-473.
[48] Tsui AK, Marsden PA, Mazer CD, Sled JG, Lee KM, Henkelman RM, Cahill LS, Zhou YQ, Chan N, Liu E and Hare GM. Differential HIF and NOS responses to acute anemia: defining organ-specific hemoglobin thresholds for tissue hypoxia. Am J Physiol Regul Integr Comp Physiol 2014; 307: R13-25.
[49] Palmer LA, Semenza GL, Stoler MH and Johns RA. Hypoxia induces type II NOS gene expression in pulmonary artery endothelial cells via HIF-1. Am J Physiol 1998; 274: L212-219.
[50] Yu JX, Cui L, Zhang QY, Chen H, Ji P, Wei HJ and Ma HY. Expression of NOS and HIF-1alpha in human colorectal carcinoma and implication in tumor angiogenesis. World J Gastroenterol 2006; 12: 4660-4664.
[51] Krishnamachary B and Semenza GL. Analysis of hypoxia-inducible factor 1alpha expression and its effects on invasion and metastasis. Methods Enzymol 2007; 435: 347-354.
[52] Luo Y, He DL, Jiang YG, Li MC, Ning L and Shen SL. Over-expression of HIF-1alpha induces EMT of human prostate cancer cells. Zhonghua Nan Ke Xue 2008; 14: 800-804.

Table S1. List of differential metabolites identified in metabolic profiling

HMDB ID	Description	Ratio	*P* value	VIP
HMDB 35586	1-Phenyl-1,3-docosanedione	9.489926393	6.73E-06	3.222033031
HMDB 38501	Polyporusterone G	7.087191163	1.76E-06	2.612538051
HMDB 29852	Methylgingerol	6.145714594	6.60E-06	2.498442822
HMDB 60754	31-Hydroxy rifabutin	5.195598454	1.07E-08	2.768869431
HMDB 61005	repaglinide aromatic amine	4.403246602	2.73E-07	2.586625334
HMDB 36638	Albigenic acid	4.325911444	2.73E-07	2.586625334
HMDB 31081	2-Pentadecanone	4.312120874	1.48E-07	2.255988512
HMDB 13198	4-O-Methylgallic acid	4.309392045	8.30E-09	2.622545254
HMDB 34408	alpha-Tocopherolquinone	4.280776346	6.38E-08	2.549242406
HMDB 61663	12-hydroxyheptadecanoic acid	4.104648263	1.97E-08	2.212591211
HMDB 01163	Guanosine diphosphate mannose	4.080933809	2.27E-06	2.215780556
HMDB 31039	Heptadecanal	3.970677167	8.53E-07	2.169015081
HMDB 14600	Prazosin	3.65858163	1.62E-06	2.06307738
HMDB 30593	Edulisin II	3.375849365	4.97E-07	2.023973182
HMDB 61658	3-hydroxyhexadecanoic acid	3.167700456	9.94E-08	2.004516932
HMDB 31829	Bisosthenon B	3.01725126	8.89E-08	2.28327881
HMDB 13643	4b-Hydroxycholesterol	2.989034863	1.59E-06	2.181685187
HMDB 29356	Feruloylglycyl-L-phenylalanine	2.885369764	1.08E-06	2.211754699
HMDB 31885	6-Hydroxypentadecanedioic acid	2.806198708	2.82E-06	2.196684971
HMDB 12642	20-Oxo-leukotriene E4	2.736872237	4.22E-09	2.187529291
HMDB 01413	Citicoline	2.708424428	2.90E-06	2.162956786
HMDB 30205	Jubanine A	2.674579446	2.19E-07	2.145917101
HMDB 38175	2-Acetyloxazole	2.595550157	2.98E-09	2.127327263
HMDB 01167	Pyruvaldehyde	2.53644422	1.24E-08	2.073931006
HMDB 31103	2-Hydroxylinolenic acid	2.471445235	1.46E-09	2.074711014
HMDB 15303	Kanamycin	2.470314186	4.44E-08	2.035234157
HMDB 33520	1-Hydroxyrutacridone epoxide	2.412478578	5.50E-10	2.051881614
HMDB 30570	Sylvopinol	2.375431063	6.17E-08	2.02529721
HMDB 32921	Ethyl 2-furanpropionate	2.343363313	7.04E-10	2.015289537
HMDB 14351	Reserpine	0.361087101	3.12E-06	2.123269492
HMDB 29068	Threoninyl-Phenylalanine	0.336936617	1.94E-10	2.274319914
HMDB 15596	Vildagliptin	0.335706828	4.34E-08	2.254471672
HMDB 60996	Acetyl-3-hydroxyprocainamide	0.330533489	6.52E-06	2.202044934
HMDB 39847	3-Oxododecanoic acid glycerides	0.321748767	3.86E-09	2.309189882
HMDB 29109	Tyrosyl-Leucine	0.316033231	1.62E-08	2.334954468
HMDB 34489	(+)-Norushinsunine N-oxide	0.307382178	6.43E-08	2.341885769
HMDB 15631	Alvimopan	0.305942027	4.27E-06	2.004306495
HMDB 33693	Falcarinone	0.298081437	1.34E-09	2.375808352
HMDB 29087	Tryptophyl-Leucine	0.296816322	8.44E-10	2.389240495
HMDB 28892	Histidinyl-Phenylalanine	0.295969813	1.05E-07	2.382403564
HMDB 33832	Cinnamyl cinnamate	0.294966946	3.22E-08	2.376479895
HMDB 28915	Isoleucyl-Proline	0.294109105	1.37E-09	2.042582624
HMDB 29129	Valyl-Histidine	0.286984366	2.89E-08	2.431229422
HMDB 29051	Serinyl-Tyrosine	0.276487998	7.00E-06	2.102208956
HMDB 28995	Phenylalanyl-Glycine	0.27532546	3.82E-11	2.11509001
HMDB 41990	Piritramide	0.273899643	2.07E-06	2.394324256
HMDB 34780	Capsiate	0.269467496	1.31E-08	2.478074054

HMDB 35292	Ganodermic acid P2	0.257257473	2.97E-06	2.518570605
HMDB 60796	6α-Hydroxy-hydromorphone	0.256425304	1.47E-08	2.526535871
HMDB 28713	Arginyl-Leucine	0.25100853	1.27E-08	2.52664011
HMDB 29097	Tryptophyl-Gamma-glutamate	0.24620323	1.43E-06	2.178438322
HMDB 13941	Epoxy-hexobarbital	0.25732824	1.80E-09	2.617520662
HMDB 28694	Alanyl-Phenylalanine	0.231146469	3.65E-09	2.633427485
HMDB 13161	2-Hexenoylcarnitine	0.226915602	5.99E-09	2.637020403
HMDB 60725	2,6-Pipecoloxylidide	0.217959219	2.65E-09	2.671322174
HMDB 13940	3'-Hydroxyhexobarbital	0.217441119	7.05E-12	2.289858042
HMDB 15444	Hexobarbital	0.215974825	3.79E-12	2.286716868
HMDB 28989	Phenylalanyl-Arginine	0.20545207	2.55E-07	2.689590703
HMDB 28940	Leucyl-Tryptophan	0.205435742	5.08E-11	2.734231635
HMDB 29005	Phenylalanyl-Threonine	0.201542081	1.87E-07	2.334205644
HMDB 29114	Tyrosyl-Serine	0.176368832	3.31E-06	2.421327248
HMDB 29093	Tryptophyl-Threonine	0.176297348	3.45E-11	2.44373297
HMDB 29027	Prolyl-Threonine	0.157263281	5.44E-07	2.875623568
HMDB 28955	Lysyl-Leucine	0.14655851	4.75E-07	2.996566246
HMDB 28888	Histidinyl-Isoleucine	0.127543124	7.28E-11	3.111443852
HMDB 37891	2-Butyl-4,5-diethyloxazole	0.113511109	5.34E-07	3.155048995
HMDB 29560	Hesperaline	0.104038662	2.35E-07	2.758747074
HMDB 01539	Asymmetric dimethylarginine	0.099577613	6.72E-08	3.287605606
HMDB 60551	Norfluoxetine	0.068910294	5.71E-06	3.039365456
HMDB 28975	Methionyl-Histidine	0.053229507	2.31E-06	3.68973167

Ratio: Differential multiple of hypoxia vs normoxia; *P* value <0.05 was considered statistically significant. *P* values were calculated using the t test; VIP: Variable Important for the Projection indicates the ratio difference of m/z contribution to PLSDA model.

Table S2. List of differentially expressed proteins identified in proteomic profiling

Accession	Description	Ratio	*P* value
PTCD3	Pentatricopeptide repeat domain-containing protein 3	0.251661104	0.008903125
HIST2H3A	Histone H3.2	0.305254414	2.26756E-05
N/A	*Highly similar to Bcl-2-like 13*	*0.378334164*	*0.002206912*
SMARCC1	SWI/SNF related, matrix associated, actin dependent regulator of chromatin, subfamily c, member 1	0.408644494	0.002740717
NDUFB1	NADH dehydrogenase ubiquinone 1	0.417316853	0.000942007
MDH1	Malate dehydrogenase, cytoplasmic	0.432984812	0.004076541
ATP6V1H	ATPase, H+ transporting, lysosomal	0.434068991	0.010427064
N/A	*Acidic ribosomal phosphoprotein P1*	*0.523414060*	*0.000590103*
H3F3B	Histone H3 (Fragment)	0.543023169	0.007956053
NEU1	Neuraminidase 1	0.550565125	0.005798506
N/A	*Highly similar to Homo sapiens solute carrier family*	*0.561108507*	*7.73155E-08*
ORMDL2	ORM1-like protein 2	0.565206457	0.000156752
SLC4A7	Anion exchange protein	0.568894891	0.000179210
LMNA	Lamin A/C	0.574863157	0.000133627
GNL3	Guanine nucleotide-binding protein-like 3	0.584127351	3.57501E-05
HIGD2A	HIG1 domain family, member 2A	0.595528518	0.013574185
NUP205	Nuclear pore complex protein Nup205	0.602365899	2.6642E-06
ARHGEF2	Rho guanine nucleotide exchange factor 2	0.612789424	0.007961447
HCG_24991	HCG24991, isoform CRA_a	0.621940214	3.65309E-05
FXR1	Fragile X mental retardation autosomal	0.623642118	0.004154078
RBM15	Putative RNA-binding protein 15	0.625807388	0.012924074
MRPL15	Ribosomal protein L15, mitochondrial	0.626177481	0.000452299
DDX5	Probable ATP-dependent RNA helicase	0.632643837	3.86984E-11

TIM17A	Mitochondrial import inner membrane translocase subunit TIM17	0.633544781	0.001138951
N/A	*Highly similar to DnaJ homolog subfamily A member 3*	*0.634421071*	*0.001147456*
BYSL	Bystin	0.636224152	2.8418E-05
CPSF7	Cleavage and polyadenylation specificity factor subunit 7	0.636795364	0.001093776
TBRG4	Transforming growth factor beta regulator 4	0.636999909	0.001363002
N/A	*Aminopeptidase*	*0.644275042*	*1.1932E-08*
KPNA2	Importin subunit alpha	0.64927833	4.9237E-05
DHX30	Putative ATP-dependent RNA helicase DHX30	0.650434357	1.54634E-05
B3KPA1	cDNA FLJ31500 fis, highly similar to Torsin A	0.650520537	0.007571957
TOP2A	DNA topoisomerase 2-alpha	0.657289794	2.57795E-06
BRIX1	Ribosome biogenesis protein BRX1 homolog	0.665175397	9.99929E-06
SLC16A3	Solute carrier family 16, member 3, isoform CRA	1.509266806	1.61898E-05
CHORDC1	Cysteine and histidine-rich domain-containing 1	1.5361851	0.000129317
PFKL	ATP-dependent phosphofructokinase, liver type	1.537441047	0.003065908
HSR1	Heat shock RNA 1	1.544219067	0.003161358
S100A2	Protein S100-A2	1.544960949	0.002352482
TUBA1A	Tubulin alpha-1A chain	1.548908731	4.37993E-06
PGAM1	Phosphoglycerate mutase	1.555351134	1.59185E-09
DPYSL2	Dihydropyrimidinase-related protein 2	1.576641376	0.000164081
HEL-S-29	Creatine kinase brain isoform 1	1.593930238	4.9412E-06
HK2	Hexokinase-2	1.617073688	0.002827695
N/A	*Highly similar to Solute carrier family 2, facilitated glucose transporter member 1*	*1.620756157*	*6.04208E-09*
MIF	Macrophage migration inhibitory factor	1.646029804	2.78827E-05
S100A4	Protein S100-A4	1.651579822	1.55327E-07
PFKP	ATP-dependent phosphofructokinase platelet	1.695085717	3.27823E-06
LRRFIP1	Leucine rich repeat interacting protein 1, isoform	1.720836483	3.81882E-05
CCDC58	Coiled-coil domain-containing protein 58	1.754331662	0.030238285
PGM1	Phosphoglucomutase-1	1.780676797	1.10263E-06
CSTB	CSTB protein	1.806851302	0.00023235
P4HA1	Prolyl 4-hydroxylase subunit α-1	1.818029271	1.39795E-11
HEL-S-68p	Phosphoglycerate kinase	1.937918696	6.40646E-09
AK4	Adenylate kinase 4, mitochondrial	1.99780736	6.09144E-10
CNN3	Calponin-3	1.99781698	9.56189E-05
ALDOC	Fructose-bisphosphate aldolase	2.108177869	3.25453E-11
PLOD2	Procollagen-lysine, 2-oxoglutarate 5-dioxygenase 2	2.117807831	2.01077E-08
FAM162A	Protein FAM162A	2.317928356	3.1065E-08
P4HA2	Prolyl 4-hydroxylase subunit alpha-2	2.449853859	1.30213E-08
N/A	*Highly similar to NDRG1*	*4.026545461*	*1.9717E-07*
N/A	*Highly similar to Homo sapiens CCAAT-box-binding transcription factor*	*8.135474324*	*0.002791993*

Ratio: Protein expression of hypoxia vs normoxia; *P* value <0.05 was considered statistically significant. *P* values were calculated using the t test. Standard for screening differential proteins: adj. *P* value <0.05 and ratio >1.5 or ratio <0.67.

Table S3. List of enriched KEGG pathways identified in proteomic profiling

Pathway_Name	*P* value	#Protein in Background	#Protein in Diff Exp
Glycolysis/Gluconeogenesis	0.000127	11	4
Galactose metabolism	0.000169	5	3
Pentose phosphate pathway	0.000332	6	3
Fructose and mannose metabolism	0.002024	3	2
Biosynthesis of amino acids	0.005186	14	3
Carbon metabolism	0.021313	23	3
Phenylalanine metabolism	0.026405	1	1
Arginine and proline metabolism	0.032372	11	2

P value <0.05 was considered statistically significant. *P* values were calculated using the t test. Protein in Diff Exp: Protein in differential expression.